Int. J. Cancer: **125**, 1328–1333 (2009)

MicroRNA regulates human vitamin D receptor

Takuya Mohri, Miki Nakajima, Shingo Takagi, Sayaka Komagata and Tsuyoshi Yokoi*

Drug Metabolism and Toxicology, Faculty of Pharmaceutical Sciences, Kanazawa University, Kakuma-machi, Kanazawa, Japan

Most of the biological effects of 1α,25-dihydroxyvitamin D_3 ($1,25(OH)_2D_3$) are elicited by the binding to vitamin D receptor (VDR), which regulates gene expression. Earlier studies reported no correlation between the VDR protein and mRNA levels, suggesting the involvement of posttranscriptional regulation. MicroRNAs (miRNAs) are small noncoding RNAs that regulate gene expression through translational repression or mRNA degradation. A potential miR-125b recognition element (MRE125b) was identified in the 3′-untranslated region of human VDR mRNA. We investigated whether VDR is regulated by miR-125b. In luciferase assays using a plasmid containing the MRE125b, the antisense oligonucleotide for miR-125b significantly increased (130% of control) the reporter activity in KGN cells, whereas the precursor for miR-125b significantly decreased (40% of control) the reporter activity in MCF-7 cells, suggesting that miR-125b functionally recognized the MRE125b. By electrophoretic mobility shift assays, it was demonstrated that the overexpression of miR-125b significantly decreased the endogenous VDR protein level in MCF-7 cells to 40% of control. $1,25(OH)_2D_3$ drastically induced the CYP24 mRNA level in MCF-7 cells, but the induction was markedly attenuated by the overexpression of miR-125b. In addition, the antiproliferative effects of $1,25(OH)_2D_3$ in MCF-7 cells were significantly abolished by the overexpression of miR-125b. These results suggest that the endogenous VDR level was repressed by miR-125b. In conclusion, we found that miR-125b posttranscriptionally regulated human VDR. Since the miR-125b level is known to be downregulated in cancer, such a decrease may result in the upregulation of VDR in cancer and augmentation of the antitumor effects of $1,25(OH)_2D_3$.

Key words: microRNA; VDR; posttranscriptional regulation

1α,25-Dihydroxyvitamin D_3 ($1,25(OH)_2D_3$ or calcitriol), a biologically active metabolite of vitamin D_3, is known as a classical regulator of calcium and bone homeostasis.[1,2] Vitamin D deficiency is linked to rickets and osteoporosis.[3] Over the last 25 years, additional roles have been found for vitamin D in the regulation of cell processes such as cell growth, differentiation and apoptosis. Accumulating evidence has revealed that vitamin D deficiency is also associated with the risk of cancer.[4] Since the vitamin D system has relevance for both the prevention and treatment of cancer,[3] the development of a number of novel synthetic vitamin D analogues as a therapeutic agent in cancer has been attempted.

Most of the biological effects of $1,25(OH)_2D_3$ are elicited by the binding to vitamin D receptor (VDR; NR1I1),[5] which belongs to the superfamily of nuclear steroid hormone receptors. After ligand binding, the VDR forms a heterodimer with retinoid X receptor (RXR; NR2B1) and binds to vitamin D responsive element (VDRE) in the regulatory region of the target genes.[6] The VDR is expressed not only in the classical vitamin D responsive organs including the intestine, bone and kidney but also in many other nonclassical vitamin D responsive organs including the liver, suggesting a broader role of the receptor.[7] It has been reported that, at the protein level, the VDR expression is higher in breast[8] and thyroid[9] cancers than in normal tissues, but no obvious difference was found in cancer and normal tissues at the mRNA level. In colon cancer, the VDR mRNA and protein expression levels are gradually increased in the early stages of cancerogenesis, but the VDR mRNA decreases subsequently to lower levels during advancement.[10] Thus, the VDR expression is upregulated in cancers, although the expression levels seem to change during disease progression and in response to therapies. However, the mechanism of the upregulation of VDR protein in cancer has not been clarified. One clue is that there is no correlation between the VDR protein and mRNA levels, suggesting the involvement of posttranscriptional regulation.

To uncover the molecular mechanism of the posttranscriptional regulation, we sought to determine whether microRNA (miRNA) might be involved in the regulation of VDR. MiRNAs are an evolutionarily conserved class of endogenous ~22-nucleotide noncoding RNAs, and play a key role in diverse biological processes, including development, cell proliferation, differentiation, apoptosis and cancer initiation and progression.[11–13] MiRNAs recognize the 3′-untranslated region (3′-UTR) of the target mRNA and cause translational repression or mRNA degradation.[14] To date, ~700 miRNAs have been identified in human, and more than one-third of all human genes have been predicted to be miRNA targets.[15] The expression of global miRNAs is deregulated in most types of human cancers.[13] In this study, we investigated the potential involvement of miRNAs in the posttranscriptional regulation of human VDR expression.

Material and methods

Chemicals and reagents

$1,25(OH)_2D_3$ was purchased from Wako Pure Chemical Industries (Osaka, Japan). The pGL3-promoter vector, phRL-TK plasmid, pT7Blue T-Vector and a dual-luciferase reporter assay system were purchased from Promega (Madison, WI). Lipofectamine2000 and LipofectAMINE RNAiMAX were from Invitrogen (Carlsbad, CA). Pre-miR miRNA Precursors for miR-125b-1 and negative control #2 were from Ambion (Austin, TX). Antisense LNA/DNA mixed oligonucleotides (AsO) for miR-125b (5′-TCACAAGTTAGGGTCTCAGGGA-3′, underlined letters are LNA) and for negative control (5′-AGAC TAGCGGTATCTTAAACC-3′) were from Greiner Japan (Tokyo, Japan). All primers and oligonucleotides were commercially synthesized at Hokkaido System Sciences (Sapporo, Japan). Antibodies to VDR (C-20) and RXRα(D-20) were from Santa Cruz Biotechnology (Santa Cruz, CA). Restriction enzymes were from Takara (Shiga, Japan), TOYOBO (Osaka, Japan) and New England Biolabs (Beverly, MA). All other chemicals and solvents were of the highest grade commercially available.

Cells and culture conditions

The human breast adenocarcinoma cell lines MCF-7 and MDA-MB-435, the human colon carcinoma cell lines LS180 and the human embryonic kidney cell line HEK293 were obtained from the American Type Culture Collection (Rockville, MD). The

Abbreviations: $1,25(OH)_2D_3$, 1α,25-dihydroxyvitamin D_3; 3′-UTR, 3′-untranslated region; AsO, antisense LNA/DNA mixed oligonucleotides; ER, estrogen receptor; miRNA, microRNA; MRE125b, miR-125b recognition element; PXR, pregnane X receptor; RXR, retinoid X receptor; VDR, vitamin D receptor; VDRE, vitamin D responsive elements.

Grant sponsor: Ministry of Health, Labor, and Welfare of Japan.

***Correspondence to:** Drug Metabolism and Toxicology, Faculty of Pharmaceutical Sciences, Kanazawa University, Kakuma-machi, Kanazawa 920-1192, Japan. Fax: +81-76-234-4407.
E-mail: tyokoi@kenroku.kanazawa-u.ac.jp

Received 17 December 2008; Accepted after revision 13 March 2009
DOI 10.1002/ijc.24459
Published online 2 April 2009 in Wiley InterScience (www.interscience.wiley.com).

human ovarian granulosa-like tumor cell line KGN[16] and the human hepatoma cell line HepG2 were obtained from Riken Gene Bank (Tsukuba, Japan). MCF-7 cells and LS180 cells were cultured in Dulbecco's modified Eagle's medium (DMEM) (Nissui Pharmaceutical, Tokyo, Japan) supplemented with 0.1 mmol/L nonessential amino acid (Invitrogen) and 10% fetal bovine serum (FBS) (Invitrogen). MDA-MB-435 cells and HepG2 cells were cultured in DMEM supplemented with 10% FBS. HEK293 cells were cultured in DMEM supplemented with 4.5 g/L glucose, 10 mmol/L HEPES and 10% FBS. KGN cells were cultured in a 1:1 mixture of DMEM and Ham's F-12 medium (Nissui Pharmaceutical) supplemented with 10% FBS. These cells were maintained at 37°C under an atmosphere of 5% CO_2-95% air.

Real-time RT-PCR for mature miR-125b

For the quantification of mature miR-125b, polyadenylation and reverse transcription were performed using an NCode miRNA First-Strand cDNA Synthesis Kit (Invitrogen) according to the manufacturer's protocol. The forward primer for miR-125b was 5′-TCC CTG AGA CCC TAA CTT GTG A-3′, and the reverse primer was the supplemented universal qPCR primer. The real-time PCR was performed using a Smart Cycler (Cepheid, Sunnyvale, CA) with Smart Cycler software (version 1.2b) as follows. After an initial denaturation at 95°C for 30 sec, the amplification was performed by denaturation at 95°C for 10 sec, annealing and extension at 60°C for 10 sec for 45 cycles.

Construction of reporter plasmids

To construct luciferase reporter plasmids, various target fragments were inserted into the *Xba*I site, downstream of the luciferase gene in the pGL3-promoter vector. The sequence from +1786 to +1813 in the human VDR mRNA (5′-CAG GAG AAA TGC ATC CAT TCC TCA GGG A-3′) was termed the miR-125b recognition element (MRE125b). The region from +1748 to +1860 containing the MRE125b in the human VDR mRNA was amplified by PCR using the following primers adapted to the *Xba*I site: 5′-TTT TCT AGA CTG CCT AAG TGG CTG CTG AC-3′ and 5′-TTT TCT AGA CGC TGG ACA AGC GGG GCC-3′. The PCR product was digested with *Xba*I and the 119-bp fragment was cloned into pGL3-promoter vector, resulting in single (pGL3/F1) and reverse single (pGL3/R1) insertions. The fragment containing 3 copies of the MRE125b, 5′-CTA GA*C AGG AGA AAT GCA TCC ATT CCT CAG GGA* CAG AG*C AGG AGA AAT GCA TCC ATT CCT CAG GGA* CAG AG*C AGG AGA AAT GCA TCC ATT CCT CAG GGA* CAG AGT-3′ (MRE125b is italicized), was cloned into the pGL3-promoter vector (pGL3/3xMRE). The complementary sequence of 3 copies of the MRE125b was also cloned into the pGL3-promoter plasmid (pGL3/3xMRE-Rev). A fragment containing the perfect matching sequence with the mature miR-125b, 5′-CTA GA*T CAC AAG TTA GGG TCT CAG GGA* T-3′ (the matching sequence of miR-125b is italicized), was cloned into the pGL3-promoter vector (pGL3/c-125b). The nucleotide sequences of the constructed plasmids were confirmed by DNA sequencing analyses.

Luciferase assay

Various luciferase reporter plasmids (pGL3) were transiently transfected with phRL-TK plasmid into MCF-7 and KGN cells. Briefly, the day before transfection, the cells were seeded into 24 well plates. After 24 hr, 450 ng of pGL3 plasmid, 50 ng of phRL-TK plasmid and the precursors for miR-125b or control were cotransfected into MCF-7 cells using LipofectAMINE 2000. For KGN cells, 450 ng of pGL3 plasmid, 50 ng of phRL-TK plasmid and the AsOs for miR-125b or control were cotransfected using LipofectAMINE 2000. After incubation for 48 hr, the cells were resuspended in passive lysis buffer and then the luciferase activity was measured with a luminometer (Wallac, Turku, Finland) using the dual-luciferase reporter assay system.

Transfection of precursor for miR-125b into MCF-7 cells and preparation of nuclear extract and total RNA

To investigate the effects of miR-125b on the expression level of VDR protein, 50 nM precursors for miR-125b or control were transfected into MCF-7 cells using LipofectAMINE RNAiMAX. After 72 hr, nuclear extract was prepared using NE-PER Nuclear and Cytoplasmic extraction reagents (Pierce, Rockford, IL) and total RNA was prepared using ISOGEN according to the manufacturer's protocols. The protein concentration in the nuclear extract was determined using Bradford protein assay reagent (Bio-Rad, Hercules, CA) with γ-globulin as a standard.

Electrophoretic mobility shift assays

Human VDR cDNA was amplified by PCR using cDNA from human normal kidney with the forward primer 5′-TCC TTC AGG GAT GGA GGC AAT GGC-3′ and the reverse primer 5′-CTG TCC TAG TCA GGA GAT CTC ATT GCC-3′. The PCR fragment was cloned into the pT7Blue T-Vector. The nucleotide sequences of the constructed plasmids were confirmed by DNA sequencing analyses. Human RXRα expression vector (pGEM-3Z/hRXRα) was previously constructed.[17] Using these plasmids and the TNT T7 Quick Coupled Transcription/Translation System (Promega), human VDR and RXRα proteins were synthesized *in vitro*. The oligonucleotide containing VDRE, 5′-aag CAC ACC cgg TGA ACT ccg-3′ (the hexamer half-sites are capitalized), was from the human *CYP24* promoter.[18] Double-stranded oligonucleotides were labeled with [γ-^{32}P]ATP using T4 polynucleotide kinase (TOYOBO) and purified by Microspin G-50 columns (GE Healthcare Bio-Sciences, Piscataway, NJ). The labeled probe (40 fmol, ~10,000 cpm) was applied to each binding reaction in 25 mM HEPES-KOH buffer (pH 7.9), 0.5 mM EDTA, 50 mM KCl, 10% glycerol, 0.5 mM dithiothreitol, 0.5 mM (*p*-amidinophenyl) methanesulfonyl fluoride, 2 μg of poly(dI-dC) and 2 μL of *in vitro* transcribed/translated proteins to a final reaction volume of 15 μL. For supershift experiments, 0.2 μg of anti-VDR antibodies or 2 μg of anti-RXRα antibodies were preincubated with *in vitro* transcribed/translated proteins or the nuclear extract at room temperature for 30 min. The mixtures were incubated on ice for 15 min and then loaded on 4% acrylamide gels in 0.5 × Tris-borate EDTA buffer. The gels were dried and then the DNA-protein complexes were detected with a Fuji Bio-Imaging Analyzer BAS 1000 (Fuji Film, Tokyo, Japan).

Real-time RT-PCR for CYP24

To investigate the effects of miR-125b on the induction of CYP24 mRNA by 1,25$(OH)_2D_3$, 50 nM precursors for miR-125b or control were transfected into MCF-7 cells using LipofectAMINE RNAiMAX. After 72 hr, the cells were treated with 100 nM 1,25$(OH)_2D_3$ (or 0.1% ethanol for control) for 24 hr. Total RNA was prepared using ISOGEN. The forward and reverse primers for CYP24 mRNA were 5′-CAG CAA ACA GTC TAA TGT GG-3′ and 5′-AGC ATA TTC ACC CAG AAC TG-3′, respectively. The real-time PCR analysis was performed as follows: after an initial denaturation at 95°C for 30 sec, the amplification was performed by denaturation at 94°C for 4 sec, annealing and extension at 62°C for 20 sec for 45 cycles. The CYP24 mRNA levels were normalized with GAPDH mRNA as described previously.[19]

Growth assay

To investigate the effects of miR-125b on the antiproliferative effects of 1,25$(OH)_2D_3$, growth assay was conducted according to the method by McGaffin *et al.*[20] with slight modifications. MCF-7 cells were plated on 96 well plates (3000 cells/well) and 20 nM precursors for miR-125b or control were transfected using LipofectAMINE RNAiMAX. After 24 hr, the cells were treated with 1 μM 1,25$(OH)_2D_3$ (or 0.1% ethanol) for 48–96 hr. The cells were rinsed with phosphate-buffered saline, fixed with 3.7% formaldehyde for 15 min and stained with 0.1% crystal violet for 10 min. The stained cells were washed with water and air dried. Crystal

violet was extracted from the stained cells with 2% sodium dodecyl sulfate, and the intensities were quantified spectrophotometrically 620 nm. The percent cell viability was calculated by comparison with the absorbance of control cells.

Statistical analyses

Data are expressed as mean ± SD of triplicate determinations. Comparison of 2 groups was made with an unpaired, two-tailed student's *t*-test. Comparison of multiple groups was made with ANOVA followed by Dunnett or Tukey test. A value of $p < 0.05$ was considered statistically significant.

Results

A miR-125b complementary sequence on the 3′-UTR of human VDR mRNA

By a computational search (http://www.targetscan.org/), several miRNAs are found to share complementarity with a sequence in the 3′-UTR of human VDR mRNA. Among them, we focused on miR-125b because its binding site is highly conserved among species (Fig. 1). The seed sequence of miR-125b was perfectly matching with the predicted binding site of the VDR mRNA. We investigated whether miR-125b might be involved in the regulation of human VDR expression through the MRE125b.

Expression levels of miR-125b in human cancer cell lines

For gain- and loss-of-function experiments, we need to know the expression level of endogenous miR-125b in cell lines. For this purpose, the expression levels of mature miR-125b in 6 kinds of human cancer cell lines were determined by real-time RT-PCR analysis. As shown in Figure 2*a*, the mature miR-125b level was highest in KGN followed by MDA-MB-435 cells, whereas it was extremely low in MCF-7, HepG2, HEK293 and LS180 cells.

Effects of overexpression or inhibition of miR-125b on luciferase activity

To investigate whether MRE125b is functional in the regulation by miR-125b, luciferase assays were performed. First, we transfected the precursor for miR-125b into MCF-7 cells in which the mature miR-125b level was low (Fig. 2*b*). Using the pGL3/c-125b plasmid containing the miR-125b complementary sequence, it was demonstrated that the luciferase activity was significantly ($p < 0.001$) decreased by the transfection of precursor for miR-125b. The luciferase activity of the pGL3/F1 plasmid was significantly ($p < 0.001$) decreased (60% of control) by the overexpression of miR-125b, but that of the pGL3/R1 plasmid was not. When the pGL3/3xMRE plasmid containing 3 copies of the MRE125b was used, a prominent suppression was observed (40% of control, $p < 0.001$) by the overexpression of miR-125b. Next, we transfected the AsO for miR-125b into KGN cells in which the mature miR-125b was highly expressed (Fig. 2*b*). The luciferase activity of the pGL3/c-125b plasmid was significantly ($p < 0.01$) lower than that of the control pGL3-p plasmid. The luciferase activity of the pGL3/c-125b plasmid was significantly ($p < 0.01$) restored by the transfection of AsO for miR-125b (3.1-fold of control). The luciferase activity of the pGL3/F1 plasmid was increased by the transfection of AsO for miR-125b, although the effects were statistically insignificant. The luciferase activity of the pGL3/3xMRE plasmid was significantly ($p < 0.01$) lower than that of the control pGL3-p plasmid. The luciferase activity of the pGL3/3xMRE plasmid was significantly (1.3-fold of control, $p < 0.05$) restored by the inhibition of miR-125b by AsO. These results suggest that miR-125b functionally recognized the MRE125b on the human VDR mRNA.

Effects of overexpression of miR-125b on the endogenous VDR protein level

We sought to examine the effects of miR-125b on the endogenous VDR protein level. When we first attempted to determine the endogenous VDR protein level in human cancer cell lines by Western blot analysis using commercially available antibodies, we could not identify the VDR protein because of multiple nonspecific bands. Therefore, we utilized electrophoretic mobility shift assays to evaluate the endogenous VDR level. The VDRE of human *CYP24* gene, which is known to be a target of VDR,[18] was used as a probe. It was confirmed that *in vitro*-synthesized VDR/RXRα heterodimers bound to the VDRE (Fig. 3*a*). With the anti-VDR or anti-RXRα antibodies, the band density of the VDR/RXRα heterodimer was decreased and the supershifted band was observed. When the probe was incubated with the nuclear extracts prepared from MCF-7 cells, the band representing the VDR/RXRα heterodimer was observed and the band density was diminished with the anti-VDR or anti-RXRα antibodies. When the precursor for miR-125b was transfected, the mature miR-125b level was prominently increased, and the band density of the VDR/RXRα heterodimer was significantly ($p < 0.001$) decreased compared with that of control (40% of control). We confirmed by Western blot analysis that the expression level of RXRα was not affected by the overexpression of miR-125b (data not shown). These results suggest that the endogenous VDR level was repressed by miR-125b.

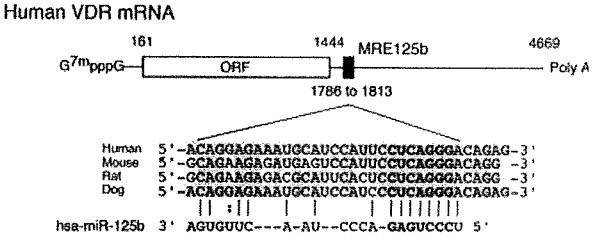

FIGURE 1 – Schematic representation of human VDR mRNA and the predicted target sequence of miR-125b. The numbering refers to the 5′ end of mRNA as 1, and the coding region is from +161 to +1444. MRE125b is located on +1786 to +1813 in the 3′-UTR of human VDR mRNA. Gray box, highly conserved regions; bold letters, seed sequence.

MiR-125b-dependent VDR regulation affects the target gene expression

We investigated whether the miR-125b-dependent regulation of VDR affects the expression of target genes. When the MCF-7 cells were treated with 100 nM $1,25(OH)_2D_3$, the CYP24 mRNA level was significantly ($p < 0.001$) increased (588-fold) (Fig. 4). However, this induction was markedly attenuated by the overexpression of miR-125b. In addition, the basal CYP24 mRNA level was also decreased by the overexpression of miR-125b, although it was statistically insignificant. These results support that the endogenous VDR level was repressed by miR-125b, and this regulation mechanism affects the expression of target genes.

Effects of overexpression of miR-125b on the antiproliferative effects of $1,25(OH)_2D_3$

We investigated the effects of miR-125b on the antiproliferative effects of $1,25(OH)_2D_3$ (Fig. 5). The cells transfected with the precursor for control were grown during incubation for 48–96 hr, but the growth was significantly ($p < 0.01$ or $p < 0.001$) reduced in the presence of 1 μM $1,25(OH)_2D_3$. Interestingly, the overexpression of miR-125b prominently ($p < 0.05$, $p < 0.01$ or $p < 0.001$) abolished the antiproliferative effects of $1,25(OH)_2D_3$. In addition, the overexpression of miR-125b could significantly ($p < 0.05$, at 96 hr) increase the cell growth in the absence of $1,25(OH)_2D_3$. These results suggest that miR-125b regulating VDR has a great impact on antiproliferative effects of $1,25(OH)_2D_3$.

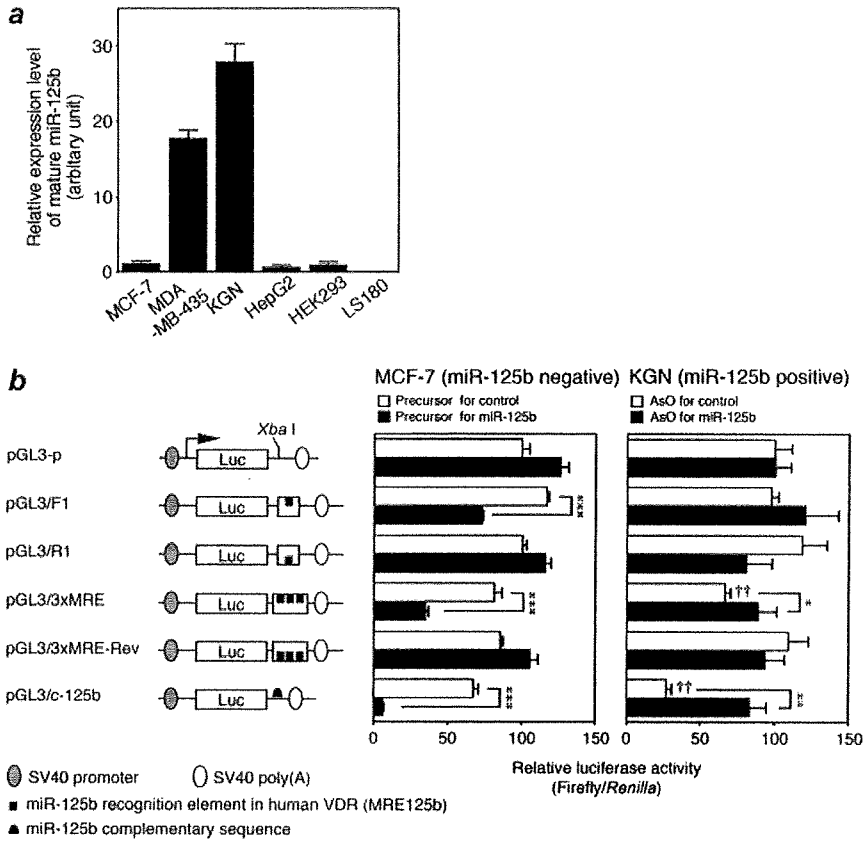

FIGURE 2 – Expression levels of mature miR-125b in various human cell lines and luciferase assays in MCF-7 and KGN cells. (*a*) The expression levels of mature miR-125b in MCF-7, MDA-MB-435, KGN, HepG2, HEK293 and LS180 cells were determined by real-time RT-PCR analysis using an NCode miRNA first-strand cDNA synthesis kit. The values were the mature miR-125b levels relative to those in MCF-7 cells. (*b*) Luciferase assays were performed to investigate whether MRE125b is functional in the regulation by miR-125b. A series of reporter constructs was transiently transfected with 10 pmol precursors for miR-125b or control into 5×10^4 MCF-7 cells, or with 5 pmol AsO for miR-125b or control into 8×10^4 KGN cells. The firefly luciferase activity for each construct was normalized with the *Renilla* luciferase activities. Values are expressed as percentages of the relative luciferase activity of pGL3-promoter plasmid. Each column represents the mean ± SD of 3 independent experiments. $*p < 0.05$, $**p < 0.01$, $***p < 0.001$, compared with the precursor or AsO for control. $\dagger\dagger p < 0.01$, compared with pGL3-p.

Discussion

In this study, we investigated whether human VDR might be regulated by miRNA. In the 3′-UTR of human VDR mRNA, a potential miR-125b recognition element (MRE125b) was identified. Luciferase assays clearly revealed that the miR-125b negatively regulated the reporter activity through MRE125b. By electrophoretic mobility shift assays and evaluation of the induction potencies of CYP24 mRNA, it was demonstrated that the endogenous VDR level was repressed by the overexpression of miR-125b. These results clearly suggest that the human VDR is post-transcriptionally regulated by miR-125b. Because the sequences of VDR mRNA around MRE125b are highly conserved among species (Fig. 1), the regulation by miR-125b may also occur in other species.

The global expression of miRNAs is deregulated in most cancer types.[21] Some studies have suggested that miRNA expression would be widely downregulated in human tumors relative to normal tissues, and other studies reported a tumor-specific mixed pattern of downregulation and upregulation of miRNA genes. Recent findings revealed that the miRNA deregulation in human cancers occurs by multiple mechanisms, including transcriptional deregulation, epigenetic alterations, mutation, DNA copy number abnormalities and dysfunction of key proteins in the miRNA biogenesis pathway.[21] Among them, alterations in DNA copy numbers would be a major mechanism because over 50% of miRNAs are in genomic fragile sites or regions associated with cancers.[12] It has been reported that miR-125b was downregulated in breast[12,22] and prostate[23] cancers. Mature miR-125b is formed by 2 precursors, miR-125b-1 and miR-125b-2. The genes for miR-125b-1 and miR-125b-2 are located in chromosome 11q24.1 and 21q11.2, respectively (http://microrna.sanger.ac.uk/sequences/). Interestingly, it has been reported that the chromosome region 11q23-24 is most frequently deleted in breast, ovarian and lung cancers[24,25] and the chromosome region 21q11-21 is frequently deleted in breast, esophagus, stomach, ovary and lung cancers.[26] This could be one of the mechanisms of the downregulation of miR-125b in cancers. Meanwhile, it is known that VDR is upregulated in several cancers,[8,9] and the upregulation appears to be associated with a good prognosis.[27] As this study demonstrated that miR-125b negatively regulated the expression of VDR, it was directly proven that the upregulation of VDR in cancers would be due to the downregulation of miR-125b.

Previously, the role of miR-125b in cell proliferation and differentiation has been reported in human prostate cancer cell lines,[28] thyroid carcinoma cells,[29] a bone marrow stroma cell line[30] and

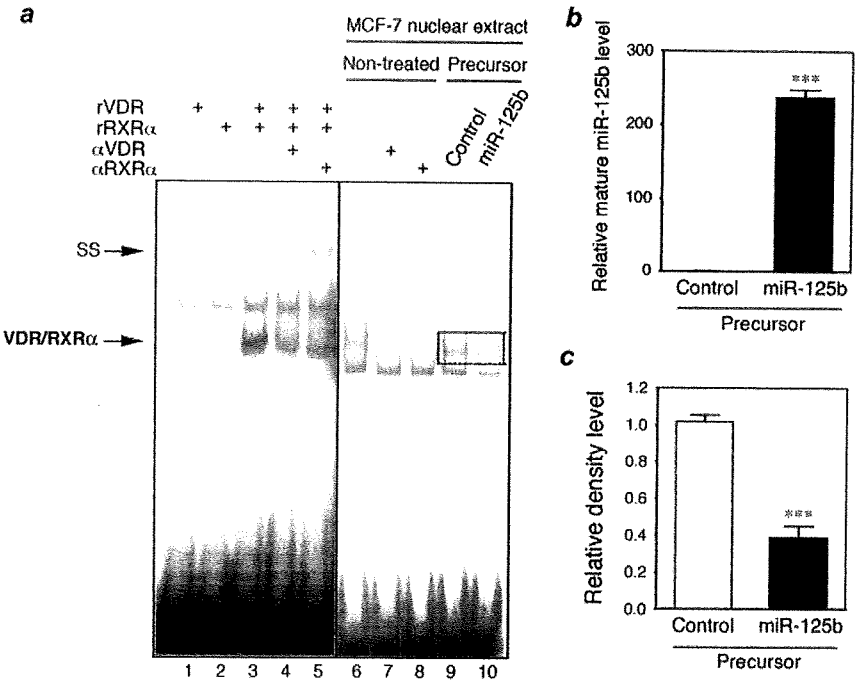

FIGURE 3 – Electrophoretic mobility shift assays to evaluate the endogenous VDR protein level. (*a*) Electrophoretic mobility shift assays were performed with oligonucleotide probe containing the VDRE in the human CYP24 promoter. The ^{32}P labeled probe was incubated with *in vitro*-synthesized VDR (rVDR) and RXRα (rRXRα) or the nuclear extract prepared from the precursors for miR-125b or control-transfected MCF-7 cells. For supershift analysis, 0.2 μg of anti-VDR antibodies (αVDR) or 2 μg of anti-RXRα antibodies (αRXRα) were preincubated with *in vitro*-synthesized proteins or the nuclear extract at room temperature for 30 min. The lower arrow indicates the VDR/RXRα-dependent shifted band and the upper arrow indicates the supershifted (SS) complex. (*b*) The mature miR-125b level was determined by real-time RT-PCR analysis. Total RNA was prepared from MCF-7 cells 72 hr after the transfection of the precursors for miR-125b or control (50 nM). The values are the mature miR-125b levels normalized with the U6 snRNA levels relative to control. (*c*) The relative density of the shifted band including VDR/RXRα complex. Each column represents the mean ± SD of 3 independent experiments. ***$p < 0.001$, compared with the precursor for control.

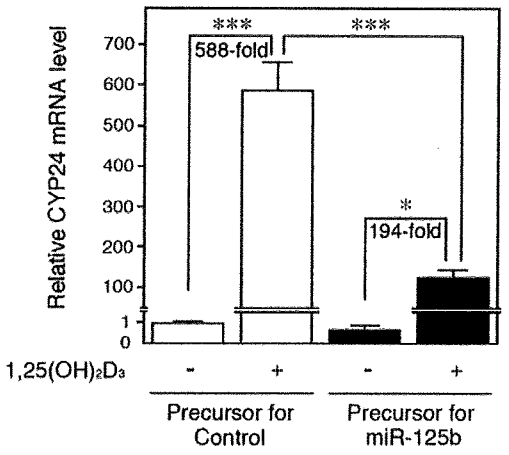

FIGURE 4 – Induction of CYP24 mRNA in MCF-7 cells by $1,25(OH)_2D_3$. The precursors for miR-125b or control (50 nM) were transfected into MCF-7 cells. After 72 hr, the cells were treated with 100 nM $1,25(OH)_2D_3$ or 0.1% ethanol (vehicle) for 24 hr and then total RNA was prepared. The CYP24 mRNA levels were determined by real-time RT-PCR and normalized with the GAPDH mRNA level. The data are expressed relative to the CYP24 mRNA level in the precursor for control-transfected cells in the absence of $1,25(OH)_2D_3$. Each column represents the mean ± SD of 3 independent experiments. *$p < 0.05$; ***$p < 0.001$.

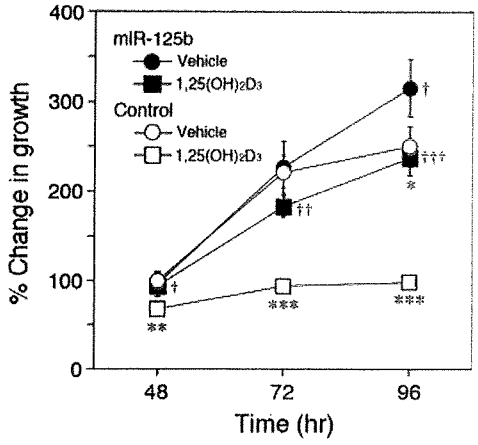

FIGURE 5 – Antiproliferative effects of $1,25(OH)_2D_3$ in MCF-7 cells. The precursors for miR-125b or control (20 nM) were transfected into MCF-7 cells. After 24 hr, the cells were treated with 1 μM $1,25(OH)_2D_3$ or 0.1% ethanol (vehicle) for 48–96 hr and then crystal violet assays were performed. Values are expressed as percentages change in growth relative to the cell viability in the precursor for control-transfected cells in the absence of $1,25(OH)_2D_3$ after 48 hr incubation. Each point represents the mean ± SD of 3 independent experiments. *$p < 0.05$, **$p < 0.01$, ***$p < 0.001$, compared with the vehicle. †$p < 0.05$, ††$p < 0.01$, †††$p < 0.001$, compared with the precursor for control.

hepatocellular carcinoma.[31] Scott *et al.*[32] reported that the miR-125b suppressed *ERBB2* and *ERBB3* oncogenes. Li *et al.*[31] reported that high expression of miR-125b was correlated with good survival in hepatocellular carcinoma patients. These previous studies suggest that miR-125b acts as a type of tumor suppressor gene. In contrast, our study demonstrated that miR-125b repressed the antiproliferative effects of $1,25(OH)_2D_3$. Thus, this study provides new information concerning the role of miR-125b in cell proliferation. In cancer cells, the downregulation of miR-125b would result in an augmentation of the antitumor effects of $1,25(OH)_2D_3$.

As regards other nuclear receptors, there are a few reports. Estrogen receptor (ER) α, which is an important marker for the prognosis and is predictive of the response to endocrine therapy in breast cancer patients, has been found to be regulated by miR-206[33] and miR-221/222.[34] These studies suggested that these miRNAs could serve as potential therapeutic targets for a subset of ERα-negative breast cancers. Previously, we found that pregnane X receptor (PXR), which is a key regulator of the expression of drug-metabolizing enzymes and transporters involved in the responses to steroids and xenobiotics, is regulated by miR-148a.[35] Thus, accumulating evidence has revealed that nuclear receptors, to which steroid hormones bind as a ligand, are regulated by miRNAs. The regulation of nuclear receptors by miRNA would result in changes in the expression of a variety of target genes, constructing complex regulatory networks.

In conclusion, we clarified that human VDR is posttranscriptionally regulated by miR-125b. This study could provide new insights into the regulatory mechanism of VDR expression.

Acknowledgements

The authors acknowledge Mr. Brent Bell for reviewing the manuscript.

References

1. Dusso AS, Brown AJ, Slatopolsky E. Vitamin D. Am J Physiol Renal Physiol 2005;289:F8–F28.
2. Nagpal S, Na S, Rathnachalam R. Noncalcemic actions of vitamin D receptor ligands. Endocr Rev 2005;26:662–87.
3. Holick MF. Vitamin D deficiency. N Engl J Med 2007;357:266–81.
4. Garland CF, Garland FC, Gorham ED, Lipkin M, Newmark H, Mohr SB, Holick MF. The role of vitamin D in cancer prevention. Am J Public Health 2006;96:252–61.
5. Carlberg C, Polly P. Gene regulation by vitamin D_3. Crit Rev Eukaryot Gene Expr 1998;8:19–42.
6. Zou A, Elgort MG, Allegretto EA. Retinoid X receptor (RXR) ligands activate the human 25-hydroxyvitamin D_3-24-hydroxylase promoter via RXR heterodimer binding to two vitamin D-responsive elements and elicit additive effects with 1,25-dihydroxyvitamin D_3. J Biol Chem 1997;272:19027–34.
7. Segura C, Alonso M, Fraga C, García-Caballero T, Diéguez C, Pérez-Fernández R. Vitamin D receptor ontogenesis in rat liver. Histochem Cell Biol 1999;112:163–7.
8. Friedrich M, Axt-Fliedner R, Villena-Heinsen C, Tilgen W, Schmidt W, Reichrath J. Analysis of vitamin D-receptor (VDR) and retinoid X-receptor α in breast cancer. Histochem J 2002;34:35–40.
9. Khadzkou K, Buchwald P, Westin G, Dralle H, Akerström G, Hellman P. 25-Hydroxyvitamin D_3 1α-hydroxylase and vitamin D receptor expression in papillary thyroid carcinoma. J Histochem Cytochem 2006;54:355–61.
10. Cross HS, Bareis P, Hofer H, Bischof MG, Bajna E, Kriwanek S, Bonner E, Peterlik M. 25-Hydroxyvitamin D_3-1α-hydroxylase and vitamin D receptor gene expression in human colonic mucosa is elevated during early cancerogenesis. Steroids 2001;66:287–92.
11. Ambros V. The functions of animal microRNAs. Nature 2004; 431:350–5.
12. Calin GA, Sevignani C, Dumitru CD, Hyslop T, Noch E, Yendamuri S, Shimizu M, Rattan S, Bullrich F, Negrini M, Croce CM. Human microRNA genes are frequently located at fragile sites and genomic regions involved in cancers. Proc Natl Acad Sci USA 2004; 101:2999–3004.
13. Lu J, Getz G, Miska EA, Alvarez-Saavedra E, Lamb J, Peck D, Sweet-Cordero A, Ebert BL, Mark RH, Ferrando AA, Downing JR, Jacks T, et al. MicroRNA expression profiles classify human cancers. Nature 2005;435:834–8.
14. Bartel DP. MicroRNAs: genomics, biogenesis, mechanism, and function. Cell 2004;116:281–97.
15. Lewis BP, Burge CB, Bartel DP. Conserved seed pairing, often flanked by adenosines, indicates that thousands of human genes are microRNA targets. Cell 2005;120:15–20.
16. Nishi Y, Yanase T, Mu YM, Oba K, Ichino I, Saito M, Nomura M, Mukasa C, Okabe T, Goto K, Takayanagi R, Kashimura Y, et al. Establishment and characterization of a steroidogenic human granulosa-like tumor cell line. KGN, that expresses functional follicle-stimulating hormone receptor. Endocrinology 2001;142:437–45.
17. Itoh M, Nakajima M, Higashi E, Yoshida R, Nagata K, Yamazoe Y, Yokoi T. Induction of human CYP2A6 is mediated by the pregnane X receptor with peroxisome proliferator-activated receptor-γ coactivator 1α. J Pharmacol Exp Ther 2006;319:693–702.
18. Chen KS, DeLuca HF. Cloning of the human 1α,25-dihydroxyvitamin D-3 24-hydroxylase gene promoter and identification of two vitamin D-responsive elements. Biochim Biophys Acta 1995;1263:1–9.
19. Tsuchiya Y, Nakajima M, Kyo S, Kanaya T, Inoue M, Yokoi T. Human CYP1B1 is regulated by estradiol via estrogen receptor. Cancer Res 2004;64:3119–25.
20. McGaffin KR, Acktinson LE, Chrysogelos SA. Growth and EGFR regulation in breast cancer cells by vitamin D and retinoid compounds. Breast Cancer Res Treat 2004;86:55–73.
21. Deng S, Calin GA, Croce CM, Coukos G, Zhang L. Mechanisms of microRNA deregulation in human cancer. Cell Cycle 2008:7:2643–6.
22. Iorio MV, Ferracin M, Liu CG, Veronese A, Spizzo R, Sabbioni S, Magri E, Pedriali M, Fabbri M, Campiglio M, Menard S, Palazzo JP, et al. MicroRNA gene expression deregulation in human breast cancer. Cancer Res 2005;65:7065–70.
23. Ozen M, Creighton CJ, Ozdemir M, Ittmann M. Widespread deregulation of microRNA expression in human prostate cancer. Oncogene 2007;27:1788–93.
24. Negrini M, Rasio D, Hampton GM, Sabbioni S, Rattan S, Carter SL, Rosenberg AL, Schwartz GF, Shiloh Y, Cavenee WK, Croce CM. Definition and refinement of chromosome 11 regions of loss of heterozygosity in breast cancer: identification of a new region at 11q23.3. Cancer Res 1995;55:3003–7.
25. Rasio D, Negrini M, Manenti G, Dragani TA, Croce CM. Loss of heterozygosity at chromosome 11q in lung adenocarcinoma: identification of three independent regions. Cancer Res 1995;55:3988–91.
26. Yamada H, Yanagisawa K, Tokumaru S, Taguchi A, Nimura Y, Osada H, Nagino M, Takahashi T. Detailed characterization of a homozygously deleted region corresponding to a candidate tumor suppressor locus at 21q11-21 in human lung cancer. Genes Chromosomes Cancer 2008;47:810–18.
27. Seubwai W, Wongkham C, Puapairoj A, Khuntikeo N, Wongkham S. Overexpression of vitamin D receptor indicates a good prognosis for cholangiocarcinoma: implications for therapeutics. Cancer 2007;109: 2497–505.
28. Lee YS, Kim HK, Chung S, Kim K-S, Dutta A. Depletion of human micro-RNA miR-125b reveals that it is critical for the proliferation of differentiated cells but not for the down-regulation of putative targets during differentiation. J Biol Chem 2005;280:16635–41.
29. Visone R, Pallante P, Vecchione A, Cirombella R, Ferracin M, Ferraro A, Volinica S, Coluzzi S, Leone V, Borbone E, Liu C-G, Petrocca F, et al. Specific microRNAs are downregulated in human thyroid anaplastic carcinomas. Oncogene 2007;26:7590–5.
30. Mizuno Y, Yagi K, Tokuzawa Y, Kanesaki-Yatsuka Y, Suda T, Katagiri T, Fukuda T, Maruyama M, Okuda A, Amemiya T, Kondoh Y, Tashiro H, et al. MiR-125b inhibits osteoblastic differentiation by down-regulation of cell proliferation. Biochem Biophys Res Commun 2008;368:267–72.
31. Li W, Xie L, He X, Li J, Tu K, Wei L, Wu J, Guo Y, Ma X, Zhang P, Pan Z, Hu X, et al. Diagnostic and prognostic implications of microRNAs in human hepatocellular carcinoma. Int J Cancer 2008;123: 1616–22.
32. Scott GK, Goga A, Berger C, Sullivan CS, Benz CC. Coordinate suppression of ERBB2 and ERBB3 by enforced expression of microRNA miR-125a or miR-125b. J Biol Chem 2007;282:1479–86.
33. Adams BD, Furneaux H, White BA. The micro-ribonucleic acid (miRNA) miR-206 targets the human estrogen receptor-α (ERα) and represses ERα messenger RNA and protein expression in breast cancer cell lines. Mol Endocrinol 2007;21:1132–47.
34. Zhao JJ, Lin J, Yang H, Kong W, He L, Ma X, Coppola D, Cheng JQ. MicroRNA-221/222 negatively regulates ERα and associates with tamoxifen resistance in breast cancer. J Biol Chem 2008;283:31079–86.
35. Takagi S, Nakajima M, Mohri T, Yokoi T. Post-transcriptional regulation of human pregnane X receptor by micro-RNA affects the expression of cytochrome P450 3A4. J Biol Chem 2008;283:9674–80.

 Basic & Clinical Pharmacology & Toxicology, **105**, 156–166

Doi: 10.1111/j.1742-7843.2009.00410.x

Identification of Urinary Biomarkers Useful for Distinguishing a Difference in Mechanism of Toxicity in Rat Model of Cholestasis

Kenji Ishihara[1], Naruo Katsutani[2], Naoki Asai[3], Akira Inomata[1], Yuji Uemura[1], Akiyoshi Suganuma[1], Kohei Sawada[1], Tsuyoshi Yokoi[4] and Toyohiko Aoki[2]

[1]Tsukuba Research, Drug Safety Research Laboratories, Eisai Co., Ltd., Tsukuba, Japan, [2]Kawashima Research, Drug Safety Research Laboratories, Eisai Co., Ltd., Kakamigahara, Japan, [3]Tsukuba Research, Analytical Research Laboratories, Eisai Co., Ltd., Tsukuba, Japan, and [4]Drug Metabolism and Toxicology, Division of Pharmaceutical Sciences, Graduate School of Medical Science, Kanazawa University, Kanazawa, Japan

(Received 19 November 2008; Accepted 14 January 2009)

Abstract: This ^{1}H nuclear magnetic resonance metabonomics study was aimed to determine urinary biomarkers of cholestasis resulting from inhibition of biliary secretion of bile or obstruction of bile flow. To inhibit biliary secretion of bile, cyclosporine A was administered to male Sprague–Dawley rats. Obstruction of bile flow was induced by administration of 4,4′-methylene dianiline, α-naphthylisothiocyanate or bile duct ligation. Clinical pathological and histopathological examinations were performed to confirm cholestatic injury and ^{1}H nuclear magnetic resonance spectral data for urine samples were analysed to determine similarities and differences in profiles of metabolites using the Spotfire®. In cyclosporine A-treated groups, serum total bilirubin and bile acid were significantly increased but no remarkable hepatic histopathological-changes were observed. In 4,4′-methylene dianiline-, α-naphthylisothiocyanate- and bile duct ligation-treated groups, serum alkaline phosphatase, γ-glutamyltranspeptidase and total bilirubin levels increased significantly, and hepatic histopathological-changes were observed. On urinary ^{1}H nuclear magnetic resonance spectral analysis, area intensities derived from 0.66 to 1.90 ppm were decreased by cyclosporine A, whereas they were increased by other treatments. These metabolites were identified using the NMR suite® as bile acids, branched-chain amino acids, n-butyrate, propionate, methyl malonate and valerate. These metabolites were further investigated by K-means clustering analysis. The cluster of these metabolites is considered to be altered by cholestasis. We conclude that bile acids, valine and methyl malonate have a possibility to be urinary cholestatic biomarkers, which distinguish a difference in mechanism of toxicity. ^{1}H nuclear magnetic resonance metabonomics thus appears to be useful for determining the mechanisms of toxicity and can be front-loaded in drug safety evaluation and biomarker discovery.

Hepatotoxicity has been a major reason for failure in drug development, particularly for new drug candidates in the preclinical stage [1,2]. Hepatotoxicity characterized mainly by arrest of bile flow is termed cholestatic injury or intrahepatic cholestasis. A variety of chemical agents can cause cholestatic injury as an idiosyncratic reaction, either immunologically or metabolically. Some are intrinsic hepatotoxins, either synthetic or natural, that lead to impairment of bile flow as a dose-dependent toxic effect. Toxic or idiosyncratic injury can interfere with bile flow by selective injury or blockade of hepatic uptake, processing or excretion of the components of bile [3].

The causes of cholestasis are classified mainly into two types, based on whether the primary injury occurs intra-hepatically (in the biliary canaliculus) or extra-hepatically (in the bile ducts). Cholestasis occurring intra-hepatically is due to interaction of chemical agents or their metabolites with transporters for excretion of the bile [4,5], while cholestasis occurring extra-hepatically is due to impairment in bile flow at the bile duct level [6,7]. Clinically, the differential diagnosis of cholestasis requires ultrasonography in addition to blood chemistry analysis and urinalysis.

One of the advantages of ^{1}H nuclear magnetic resonance-based metabonomics is its ability to quickly and stably detect a wide range of metabolites with various physicochemical properties in biofluids [8,9]. It can thus provide information on changes in biological substances associated with cholestasis by a single measurement with clustering and pattern detection analysis [10]. ^{1}H nuclear magnetic resonance-based metabonomics can be used for a wide range of problems, including disease diagnosis, preclinical evaluation of candidate drugs in safety studies, assessment of safety in humans in clinical trials, and nutritional studies [11]. However, ^{1}H nuclear magnetic resonance-based metabonomics has not been successfully applied to early diagnosis of cholestasis, because the validity of biomarkers in urine has not been well-established.

In a previous ^{1}H nuclear magnetic resonance metabonomics study, we investigated and compared the biochemical profiles of metabolites in urine from rats treated with hepatotoxicants with different mechanisms of effect [12]. We used 4,4′-methylene dianiline as a model compound inducing bile duct injury, and clofibrate and galactosamine to produce models of

Author for correspondence: Kenji Ishihara, Tsukuba Research, Drug Safety Research Laboratories, Eisai Co., Ltd., 5-1-3 Tokodai, Tsukuba 300-2635, Japan (fax + 81 29 847 6931, e-mail k3-ishihara@hhc.eisai.co.jp).

peroxisome proliferation in the liver and hepatocyte death, respectively [12]. The most significant differences between the 4,4′-methylene dianiline-treated groups (250 mg/kg oral administration) and groups treated with other agents (clofibrate 500 mg/kg oral administration, galactosamine 500 mg/kg intraperitoneal administration) were observed in chemical shifts of peaks mainly between 0.66 and 1.90 ppm. These findings suggested that ^{1}H nuclear magnetic resonance analysis of these urinary metabolites may provide a powerful means of determination of the pathophysiological status of cholestasis induced by hepatotoxicants such as cyclosporine A, 4,4′-methylene dianiline and α-naphthylisothiocyanate.

The purpose of the present study was to determine whether ^{1}H nuclear magnetic resonance-based metabonomics using urine samples can discriminate differences in mechanism of toxicity after administration of chemical agents or treatment causing cholestatic injury. To inhibit biliary secretion of bile acid, cyclosporine A was administered to male Sprague–Dawley (Crl : CD(SD)) rats. Obstruction of bile flow was induced by administration of 4,4′-methylene dianiline or α-naphthylisothiocyanate. In addition, artificial cholestasis to obstruct bile flow was induced by bile duct ligation in rats. To identify putative metabolites associated with cholestasis, urine samples obtained were subjected to ^{1}H nuclear magnetic resonance analysis along with clinical pathological and histopathological examinations to confirm cholestatic injury.

Materials and Methods

Test materials and animal treatment. Cyclosporine A (Sandimmun®) as a solution (50 mg/ml) for intravenous administration was obtained from Novartis pharma (East Hanover, NJ, USA). For intraperitoneal administration, cyclosporine A was diluted with saline solution. 4,4′-methylene dianiline and α-naphthylisothiocyanate were obtained from Sigma-Aldrich (St Louis, MO, USA). They were suspended in 0.5% methylcellulose solution. All other reagents and chemicals for the nuclear magnetic resonance experiments and biochemical analyses were of the highest commercially available quality.

Fifty-six male Crl : CD(SD) rats (Charles River Japan, Shiga, Japan) were divided into a total of 12 groups, including 10 groups (n = 5) for cyclosporine A, 4,4′-methylene dianiline, α-naphthylisothiocyanate treatment and two groups (n = 3) for bile duct ligation. The animals were kept individually in metabolic cages at a temperature of 23 ± 3° with 55 ± 20% relative humidity and a 12 hr light/12 hr dark cycle with at least 10 air changes per hour. They were allowed to access solid CDF-1 rodent chow (Oriental Yeast, Tokyo, Japan) and water *ad libitum*.

At 8 weeks of age, four groups of rats of the same age received a single oral administration of 4,4′-methylene dianiline (50: minimum toxic dose [13], 100 or 250 mg/kg, n = 5) or vehicle (0.5% methylcellulose solution, n = 5) as control-1. Three groups of animals received repeated intraperitoneal administration of cyclosporine A (10 or 20 mg/kg/day for 14 days, n = 5) or vehicle (saline solution, n = 5) as control-2. The dose and period of administration of cyclosporine A were selected based on previous studies [14–16]. Other groups of rats received a single oral administration of 4,4′-methylene dianiline (75 mg/kg, n = 5), α-naphthylisothiocyanate (75 mg/kg, n = 5) or vehicle (0.5% methylcellulose solution, n = 5) as control-3. Under anaesthesia with pentobarbital, the common bile duct was ligated (n = 3). Control animals underwent sham operation (control-4, n = 3).

This study was approved by the Eisai Laboratory Animal Care and Use Committee. All experiments were carried out in accordance with the Guiding Principles for the Care and Use of Laboratory Animals adopted by the Japanese Pharmacological Society, and Eisai's guidelines on animal experimentation (Eisai, Japan). Every effort was made to reduce the number of animals used in the study and to minimize their suffering.

Clinical pathology and histopathology. Blood samples (0.3 ml) were collected from the tail vein prior to administration and 4, 7, and 14 days after administration in the cyclosporine A-treated groups; at 8 hrs and 1, 2, and 4 days after administration in the 4,4′-methylene dianiline- and α-naphthylisothiocyanate-treated groups; and prior to treatment and 2 and 4 days after treatment in the bile duct ligation groups. Serum levels of alkaline phosphatase, alanine aminotransferase, aspartate aminotransferase, γ-glutamyltranspeptidase, total bilirubin, and total bile acids (except in the 4,4′-methylene dianiline/α-naphthylisothiocyanate-treated groups) and biochemical markers of renal function (urea nitrogen and creatinine) were measured with a 7180 automated analyser (Hitachi, Tokyo, Japan) using appropriate kits. Dunnett's tests were used to compare clinical chemical data among groups.

Animals were euthanized by exsanguination under isoflurane anaesthesia and necropsied on the last day. The liver and kidneys were collected and fixed in neutral-buffered 10% formalin and were processed for microscopic examination of routine-paraffin embedded sections stained with haematoxylin and eosin.

Urine collection and ^{1}H nuclear magnetic resonance measurement. Twenty-four-hour urine samples were collected to analyse day-to-day change in urinary metabolites because the treatment (cyclosporine A, 4,4′-methylene dianiline, α-naphthylisothiocyanate and bile duct ligation) employed in this study causes cholestatic injury lasting more than 4 days. Urine samples were collected in a flask containing 1% sodium azide from rats housed in metabolic cages during the following periods: in the 4,4′-methylene dianiline-treated groups (50, 100, and 250 mg/kg), from pre-administration to 3 days after administration; from pre-administration to 14 days after administration in the cyclosporine A-treated groups; pre-administration and 0–4 hr, 4–8 hr, 8–24 hr, 1–2 days, 2–3 days, and 3–4 days after administration in the 4,4′-methylene dianiline (75 mg/kg) and α-naphthylisothiocyanate-treated groups; and from pre-treatment to 4 days after treatment in the bile duct ligation groups. Samples were frozen at −20° until nuclear magnetic resonance spectroscopic analysis.

To minimize pH variation in the urine samples, 300 μl of buffer solution (0.2 M Na_2HPO_4/0.2 M NaH_2PO_4, pH 7.41) was mixed with 600 μl aliquots of urine. One hundred microlitres of 11 mM 3-(trimethylsilyl)propionic-2,2,3,3-d_4 acid sodium salt (as an internal chemical shift reference at 0.00 ppm) in D_2O (for field-frequency lock) was added, and the resulting solution was left to stand for 10 min. Samples were centrifuged at 15,490 ×*g* for 10 min. at 10° to remove any precipitates. The supernatant (650 μl) was placed in a 5 mm glass-tube (Wako Pure Chemical Industries, Osaka, Japan) and analysed at 298 K by ^{1}H nuclear magnetic resonance spectroscopy at 600.13 MHz using a Bruker AVANCE 600 spectrometer (Bruker Biospin, Rheinstetten, Germany). In total, 16 transients were collected into 64 K data points using the 1D-NOESY pulse sequence with solvent presaturation at the water frequency during relaxation delay (5 s) and a mixing time (t_m) of 100 ms. Summed free induction decays were multiplied by an exponential weighting function corresponding to a line broadening of 0.3 Hz before Fourier transformation. Fourier-transformed ^{1}H nuclear magnetic resonance spectra were manually phased, baseline-corrected and referenced to 3-(trimethylsilyl)-propionic 2,2,3,3-d_4 acid sodium salt (0.00 ppm) using TOPSPIN (version 2.0, Bruker).

Data reduction, clustering and pattern detection analysis of ^{1}H nuclear magnetic resonance spectral data and metabolite identification. Each spectrum recorded was reduced to 202 integrated regions of equal

width (0.04 ppm) corresponding to the region 0.42–10.00 ppm using AMIX (version 3.5, Bruker). The area for each segmented region was expressed as an integral value, resulting in an intensity distribution description of the entire spectrum with 202 variables. The region between 6.00 and 4.50 ppm was set to zero integral in order to remove effects of variation in the suppression of water resonance and the effects of variation in the urea signal caused by partial saturation via solvent-exchanging protons. To avoid including parent and metabolised drugs in the analysis, certain regions of the nuclear magnetic resonance spectra were omitted. For 4,4′-methylene dianiline the spectral peaks at 6.82, 6.46, and 3.78 ppm were removed [17], for α-naphthylisothiocyanate the aromatic regions were omitted [8], and for cyclosporine A the spectral peak at 3.70 ppm was removed [18]. All remaining spectral segments were scaled to the total integrated area of the spectrum to reduce variation in concentration. These data were collected into Excel (Microsoft, Excel 2003, SP2) data tables, in which each row included the integral descriptors for an nuclear magnetic resonance spectrum.

The signal pulse and nuclear magnetic resonance spectral data sets were imported into the Spotfire® Decision Site 8.1.1 software package (Tibco Software, CA, USA). For pattern detection, heat-map analysis was performed to characterize and to verify area intensities of these spectral chemical shifts. Chemical shifts considered to be induced by treatment were then clustered by pattern of alteration using K-means clustering analysis, a type of non-hierarchical clustering.

Based on these analyses, candidate metabolites in urine were identified by the NMR suite® (version 5.1, Chenomx, Alberta, Canada) [19], which has a database of about 200 pure compounds to analyse the 1D nuclear magnetic resonance spectra, and can compare the spectral signatures to those found in the urine spectrum and give quantitative metabolic profiles [20–23]. We also referred to data in the literature [24–26] for the assignment of metabolites, ensuring recognition of patterns of change in metabolites over time.

Dunnett's tests were used to compare area intensity of chemical shift data among groups.

Results

Changes in metabolites in 4,4′-methylene dianiline (50, 100, and 250 mg/kg) treatment groups.

Changes in clinical pathological parameters of 4,4′-methylene dianiline-treated groups (50, 100, and 250 mg/kg) are shown in table 1. From the 50 mg/kg (minimum toxic dose) dose group, 4,4′-methylene dianiline treatment elevated serum levels of alanine aminotransferase, aspartate aminotransferase, γ-glutamyltranspeptidase and total bilirubin above values in the control. Urine nuclear magnetic resonance spectra were

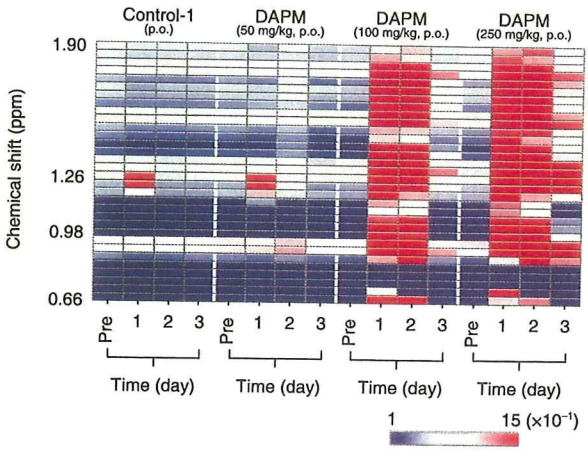

Fig. 1. Clustered heat-map for urinary metabolite nuclear magnetic resonance (NMR) following administration of 4,4′-methylene dianiline (DAPM, 50, 100, and 250 mg/kg, oral administration, n = 5/dose group) and control (Control-1: 0.5% methylcellulose solution, oral administration, n = 5) animals. The colours of the heat map represent the area intensity of chemical shifts from 0.66 to 1.90 ppm: blue for low, white for intermediate and red for high area intensity.

further examined by heat-map analysis using the Spotfire®, which revealed that the area intensity of proton signals from 0.66 to 1.90 ppm increased in a dose-dependent manner (fig. 1). The endogenous metabolites that were increased in 4,4′-methylene dianiline-treated groups as observed on ^{1}H nuclear magnetic resonance analysis of urine were identified using the NMR suite® and summarized in table 2. Metabolites corresponding to chemical shifts in the region 0.66 to 1.90 ppm included bile acids, branched-chain amino acids (isoleucine, leucine, and valine) and catabolites of branched-chain amino acids. Pattern detection by K-means clustering analysis (fig. 2) revealed that bile acids (fig. 2A), valine (fig. 2B) and methyl malonate (fig. 2C) in urine increased dose-dependently and significantly at doses of 100 and 250 mg/kg after treatment with 4,4′-methylene dianiline. We have also measured the concentration of bile acids in urine samples by LC/MS/MS

Table 1.

Changes in serum biochemistry parameters of rats given 4,4′-methylene dianiline (DAPM).

	Control-1 p.o., 0.5% methyl cellulose	DAPM p.o., 50 mg/kg		DAPM p.o., 100 mg/kg		DAPM p.o., 250 mg/kg	
Group	Total	1-day	2-day	1-day	2-day	1-day	2-day
ALP (mU/ml)	972 ± 144	946 ± 190	1047 ± 343	2318 ± 1168[1]	2498 ± 852[1]	3593 ± 1491[1]	4086 ± 1456[1]
ALT (mU/ml)	42 ± 5	141 ± 190	350 ± 425[1]	611 ± 289[1]	1894 ± 406[1]	1018 ± 148[1]	1992 ± 764[1]
AST (mU/ml)	112 ± 19	198 ± 170	392 ± 387[1]	933 ± 388[1]	3015 ± 1431[1]	1353 ± 264[1]	3418 ± 1623[1]
GGT (mU/ml)	1 ± 1	1 ± 1	2 ± 1[1]	12 ± 5[1]	15 ± 5[1]	8 ± 2[1]	5 ± 4[1]
Total bilirubin (mg/dl)	0.06 ± 0.02	0.33 ± 0.47[1]	0.29 ± 0.46[1]	3.11 ± 1.70[1]	9.72 ± 5.01[1]	3.79 ± 1.33[1]	11.18 ± 1.80[1]

ALP, alkaline phosphatase; ALT, alanine aminotransferase; AST, aspartate aminotransferase; GGT, γ-glutamyltranspeptidase; p.o., oral administration.

Results are expressed as means ± S.D. of five animals.

[1]Significantly different from control-1 ($P < 0.05$).

Table 2.
The endogenous metabolites increased in the 4,4′-methylene dianiline-treated group observed in the ^{1}H nuclear magnetic resonance analysis of rat urine.

Chemical shift (ppm)	Metabolite[1]
0.66, 0.70, 1.34, 1.38, 1.62, 1.66, 1.74	Bile acid (cholate)
0.90, 1.10	Isoleucine
0.90, 1.58	n-butyrate
0.94, 1.70	Leucine
0.98, 1.02	Valine
1.06	Propionate
1.22	Methyl malonate
1.26	3-Hydroxyisovalerate
1.30	Valerate
1.46	Alanine
7.98, 8.02	Amide NH-signals of conjugated bile acid

[1]Candidate metabolites were identified by the NMR suite® [19], as well as assignments on the basis of data in the literature [24–26].

method in 4,4′-methylene dianiline experiments, and confirmed that there is a dose-dependent increase in concentration of urinary bile acids, and a good correlation between results obtained with nuclear magnetic resonance and LC/MS/MS methods (data not shown).

Clinical pathology.
Changes in clinical pathological parameters in the cyclosporine A-, 4,4′-methylene dianiline-, α-naphthylisothiocyanate- and bile duct ligation-treated groups are presented in table 3. The dose of 4,4′-methylene dianiline 75 mg/kg was selected to induce moderate toxicological changes. In the cyclosporine A-treated group (upper, table 3), decreases in serum levels of alkaline phosphatase, alanine aminotransferase, and aspartate aminotransferase were observed in the 20 mg/kg dose group from 4 days. Serum level of aspartate aminotransferase in the 10 mg/kg dose group decreased from 7 days. Only the 10 mg/kg dose group exhibited a statistically significant increase in γ-glutamyltranspeptidase. In animals treated with cyclosporine A, serum total bilirubin and total bile acid levels increased significantly from 4 days, by about 3–4 times and 10–19 times, respectively. In the 4,4′-methylene dianiline-, α-naphthylisothiocyanate- and bile duct ligation-treated groups (middle and bottom of table 3), serum levels of alkaline phosphatase, alanine aminotransferase, aspartate aminotransferase, γ-glutamyltranspeptidase, and total bilirubin increased significantly, with peaks at 1 or 2 days after treatment, exhibiting the features of cholestasis.

There were no significant changes in renal function parameters in any (cyclosporine A, 4,4′-methylene dianiline, α-naphthylisothiocyanate or bile duct ligation) of the treated groups (data not shown).

Histopathology.
Pathological findings in rats are presented in table 4. No remarkable hepatic histological changes were observed in the control group or the group treated with cyclosporine A

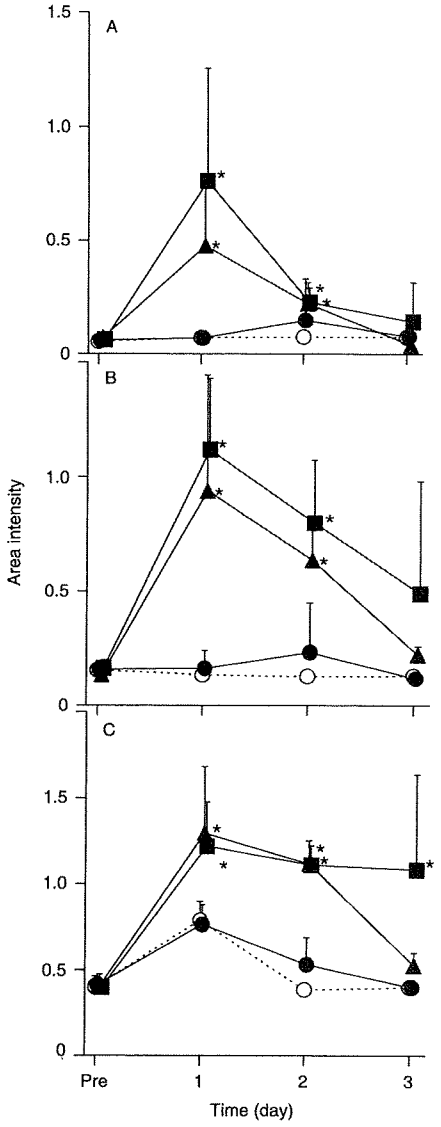

Fig. 2. Change in mean area intensity of chemical shifts for bile acids (A), valine (B) and methyl malonate (C). Animals treated with: vehicle (○: 0.5% methylcellulose solution, oral administration) or 4,4′-methylene dianiline (DAPM, ●: 50 mg/kg, ▲: 100 mg/kg, or ■: 250 mg/kg, oral administration). Each point represents means ± S.D. of five animals. Significant difference from the control group, *P < 0.05.

for 14 days. In the 4,4′-methylene dianiline-treated group, hepatic changes characterized by exfoliated necrotic of biliary epithelial cells and necrosis of hepatocyte were observed after 8 hrs, and bile duct hyperplasia, periportal inflammation with oedema and fibrosis were observed after 1 and 4 days. In the α-naphthylisothiocyanate-treated group, hepatic changes characterized by bile duct hyperplasia and fibrosis in the periportal area were observed. In the bile duct ligation-treated group, bile duct changes characterised by bile duct hyperplasia, periportal inflammation, and fibrosis and necrosis of hepatocyte were observed.

Table 3.

Changes in serum biochemistry parameters of rats given cyclosporine A (CyA), 4,4′-methylene dianiline (DAPM), a-naphthylisothiocyanate (ANIT) or bile duct ligation (BDL).

Group	Control-2	CyA (i.p., 10 mg/kg)				CyA (i.p., 20 mg/kg)			
	Total	Pre	4-day	7-day	14-day	Pre	4-day	7-day	14-day
ALP (mU/ml)	1437 ± 350	1536 ± 258	1238 ± 218	1418 ± 322	1264 ± 316	1302 ± 225	997 ± 189[1]	1181 ± 384	859 ± 90[1]
ALT (mU/ml)	42 ± 8	41 ± 3	34 ± 2	33 ± 2	43 ± 4	42 ± 5	32 ± 4[1]	32 ± 4a	34 ± 8
AST (mU/ml)	91 ± 6	104 ± 14	86 ± 11	62 ± 4[1]	67 ± 8[1]	96 ± 12	65 ± 7[1]	62 ± 18[1]	56 ± 6[1]
GGT (mU/ml)	1 ± 1	1 ± 0	0 ± 1	2 ± 0[1]	1 ± 0	1 ± 0	0 ± 0	1 ± 0	1 ± 0
Total bilirubin (mg/dl)	0.05 ± 0.01	0.06 ± 0.00	0.14 ± 0.03[1]	0.16 ± 0.01[1]	0.14 ± 0.01[1]	0.04 ± 0.01	0.15 ± 0.03[1]	0.19 ± 0.03[1]	0.17 ± 0.03[1]
Total bile acid (μmol/l)	6.2 ± 4.4	9.1 ± 6.1	113.0 ± 64.0[1]	97.0 ± 48.7[1]	60.1 ± 60.0[1]	4.1 ± 0.3	66.5 ± 53.4[1]	103.4 ± 42.6[1]	88.4 ± 46.2[1]

Group	Control-3	DAPM (p.o., 75 mg/kg)				ANIT (p.o., 75 mg/kg)			
	Total	8 hrs	1-day	2-day	4-day	8 hrs	1-day	2-day	4-day
ALP (mU/ml)	1508 ± 391	1105 ± 157	3871 ± 770[2]	3343 ± 1206[2]	2033 ± 363[2]	1315 ± 214	1281 ± 142	2361 ± 317[2]	1842 ± 256
ALT (mU/ml)	47 ± 6	57 ± 23	473 ± 169[2]	850 ± 433[2]	68 ± 9	47 ± 6	94 ± 31	1049 ± 386[2]	139 ± 31[2]
AST (mU/ml)	107 ± 20	169 ± 62	770 ± 280[2]	1139 ± 680[2]	81 ± 8	95 ± 10	204 ± 55[2]	2056 ± 995[2]	155 ± 33[2]
GGT (mU/ml)	1 ± 1	3 ± 2[2]	11 ± 3[2]	9 ± 4[2]	1 ± 1	1 ± 0	5 ± 3[2]	6 ± 0[2]	1 ± 0
Total bilirubin (mg/dl)	0.06 ± 0.02	0.22 ± 0.10[2]	2.68 ± 0.38[2]	5.65 ± 2.82[2]	0.51 ± 0.11[2]	0.09 ± 0.04	0.87 ± 0.58[2]	6.73 ± 1.67[2]	1.06 ± 0.38[2]
Total bile acid (μmol/l)	–	169.9[3]	521.8[3]	–	–	–	–	–	–

Group	Control-4	BDL		
	Total	Pre	2-day	4-day
ALP (mU/ml)	573 ± 209	672 ± 126	2948 ± 768[4]	1281 ± 288[4]
ALT (mU/ml)	37 ± 24	32 ± 2	1565 ± 625[4]	445 ± 184[4]
AST (mU/ml)	89 ± 35	119 ± 8	2219 ± 383[4]	970 ± 32[4]
GGT (mU/ml)	1 ± 1	0 ± 0	7 ± 6[4]	11 ± 8[4]
Total bilirubin (mg/dl)	0.07 ± 0.01	0.07 ± 0.01	9.07 ± 3.03[4]	14.76 ± 10.14[4]
Total bile acid (μmol/l)	13.1 ± 7.4	7.2 ± 4.8	198.4 ± 164.0[4]	153.5 ± 13.2[4]

ALP, alkaline phosphatase; ALT, alanine aminotransferase; AST, aspartate aminotransferase; GGT, γ-glutamyltranspeptidase; Control-2, intraperitoneal administration (i.p.), saline solution; Control-3, oral administration (p.o.), 0.5% methyl cellulose; Control-4, sham operation; –, Not measured. Results are expressed as means ± S.D. of five (CyA, ANIT, and DAPM groups) or three (BDL groups) animals.

[1]Significantly different from Control-2 ($P < 0.05$).

[2]Significantly different from Control-3 ($P < 0.05$).

[3]Means of two animals.

[4]Significantly different from Control-4 ($P < 0.05$).

 Basic & Clinical Pharmacology & Toxicology, **105**, 156–166

Table 4.

Pathological findings of rats given cyclosporine A (CyA), 4,4′-methylene dianiline (DAPM), a-naphthylisothiocyanate (ANIT) or bile duct ligation (BDL).

		CyA				DAPM			ANIT	BDL
		10 mg/kg		20 mg/kg		75 mg/kg			75 mg/kg	
Organ	Pathological findings	7 day	14 day	7 day	14 day	8hr	1 day	4 day	4 day	4 day
Liver	Necrosis, biliary epithelial cell	–	–	–	–	1+	1+	–	–	–
	Periportal inflammation	–	–	–	–	–	1+	1+	–	1+
	Periportal fibrosis	–	–	–	–	–	–	2+	1+	1+
	Hyperplasia, bile duct	–	–	–	–	–	1+	1+	1+	2+
	Necrosis, hepatocyte	–	–	–	–	1+	1+	1+	–	1+
Kidney	Tubular degeneration	1+	1+	2+	3+	–	–	–	–	–

Grade: –, No histopathological changes; 1+, slight; 2+, moderate; 3+, marked.

In the cyclosporine A-treated group, histological changes characterised by tubular degeneration of kidney were noted. There were no renal pathological changes in the 4,4′-methylene dianiline-, α-naphthylisothiocyanate- or bile duct ligation-treated groups.

^1H nuclear magnetic resonance spectral analysis of urine samples.

Changes in peaks in the cyclosporine A-, 4,4′-methylene dianiline-, α-naphthylisothiocyanate- and bile duct ligation-treated groups were evaluated by heat-map clustering (fig. 3).

In the cyclosporine A-treated groups, area intensities of the region 0.66 to 1.90 ppm were suppressed from 6 days (20 mg/kg) or 7 days (10 mg/kg) of administration to the end of the 14-day treatment period, but were enhanced after treatment with 4,4′-methylene dianiline (75 mg/kg), α-naphthylisothiocyanate and bile duct ligation.

Chemical shifts of peaks induced by treatment with cyclosporine A, 4,4′-methylene dianiline, α-naphthylisothiocyanate or bile duct ligation were clustered by pattern of alteration, as determined by K-means clustering analysis. Seven characteristic clusters of changes were found among all treated

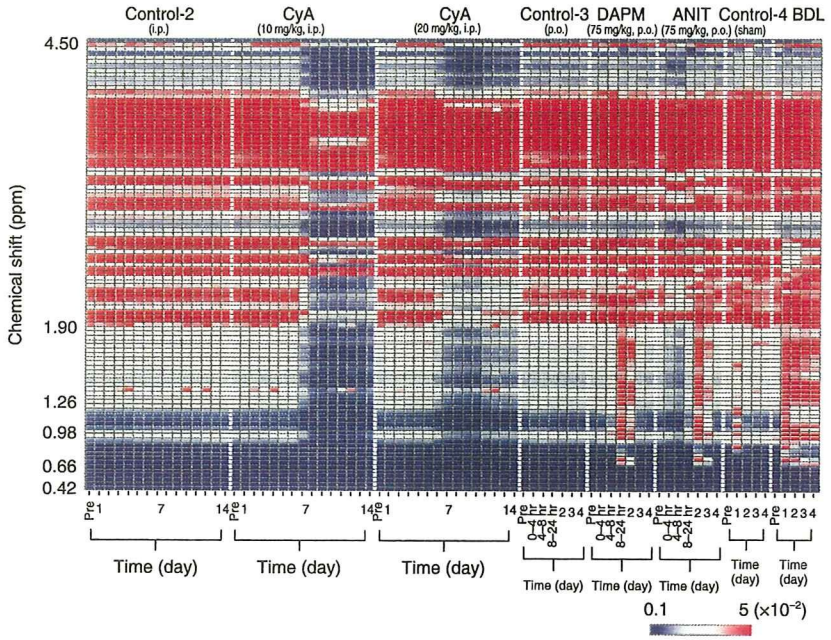

Fig. 3. Clustered heat-map for urinary metabolite nuclear magnetic resonance (NMR) following administration of cyclosporine A (CyA, 10 and 20 mg/kg, intraperitoneal administration, n = 5), 4,4′-methylene dianiline (DAPM, 75 mg/kg, oral administration, n = 5), α-naphthylisothiocyanate (ANIT, 75 mg/kg, oral administration, n = 5) or bile duct ligation (BDL, n = 3) and control (Control-2: saline solution, intraperitoneal administration, n = 5; Control-3: 0.5% methyl cellulose, oral administration, n = 5; Control-4: sham operation, n = 3) animals. The colours of the heat map represent the area intensity of chemical shifts from 0.42 to 4.50 ppm: blue for low, white for intermediate and red for high area intensity.

Table 5.

The endogenous metabolites of rat urine induced by treatment with cyclosporine A, 4,4′-methylene dianiline, a-naphthylisothiocyanate or bile duct ligation were clustered by pattern of alteration using K-means clustering analysis.

Cluster	Chemical shift (ppm)	Metabolite[1]
Cluster 1	2.42	Succinate
	2.46, 3.02	2-Oxyglutarate
	2.50, 2.54, 2.66	Citrate
	2.70	Sarcosine
	6.54	Fumarate
	3.98, 7.54, 7.58, 7.62, 7.66, 7.82, 7.86	Hippurate
Cluster 2	7.10	Histidine
	7.18	Tyrosine
	7.22, 7.30, 7.34	Tryptophan
	7.26	3-Indoxyl sulphate
	7.38, 7.42	Phenylalanine
Cluster 3	2.06, 3.34, 4.14	Proline
	2.26, 3.66	Acetoacetate
	2.86	*N,N*-dimethylglycine
	4.02, 4.50	Ascorbate
	4.06	Creatinine
	4.26	Threonine
	4.30, 6.10	Adenosine
	6.86, 7.70	4-aminohippurate
	8.46	Formate
Cluster 4	3.22, 3.38, 3.46, 3.50, 3.54, 3.74, 3.82, 3.86	Glucose
	3.26	Trimethylamine-*N*-oxide
	3.42	Taurine
	3.90	Betaine
Cluster 5	0.66, 0.70, 1.34, 1.38, 1.62, 1.66, 1.74	Bile acid (cholate)
	0.90, 1.10	Isoleucine
	0.90, 1.58	n-butyrate
	0.94, 1.70	Leucine
	0.98, 1.02	Valine
	1.06	Propionate
	1.22	Methyl malonate
	1.26	3-hydroxyisovalerate
	1.30	Valerate
	1.46	Alanine
	7.98, 8.02	Amide NH-signals of conjugated bile acid
Cluster 6	1.78, 1.82, 1.86, 3.10	Ornithine
	1.90	Acetate
	1.98, 2.10, 2.14, 2.18, 2.34, 2.38	Homoserine
Cluster 7	8.90, 8.98, 9.26	*N*-methylnicotinamide

[1]Candidate metabolites were identified by the NMR suite® [19], as well as assignments on the basis of data in the literature [24–26].

groups and candidate metabolites were identified (table 5). Changes in mean area intensity of chemical shifts about clusters are shown in figs 4 and 5. The first cluster, including sarcosine, represented the area intensity of chemical shifts unchanged from 1 to 6 days of administration and suppressed thereafter in the cyclosporine A-treated groups (fig. 4A), as well as those suppressed by treatment with 4,4′-methylene dianiline, α-naphthylisothiocyanate or bile duct ligation (fig. 4B). The second one, which included histidine, represented the area intensity of chemical shifts unchanged after cyclosporine A treatment (fig. 4C) and those transiently enhanced and peaking at 24-hr post-administration in the 4,4′-methylene dianiline-treated group (fig. 4D). The third one, which included acetoacetate, represented the area intensity of chemical shifts enhanced from 1 to 6 days of administration in the cyclosporine A-treated group (fig. 4E) and those enhanced by treatment with 4,4′-methylene dianiline and α-naphthylisothiocyanate, but unchanged in the bile duct ligation-treated group (fig. 4F). The fourth one, which included glucose, represented the area intensity of chemical shifts increased in the cyclosporine A-treated groups (fig. 4G) and transiently increased in the α-naphthylisothiocyanate-treated group (fig. 4H).

The fifth cluster included bile acids, valine and methyl malonate (fig. 5). Other metabolites belonging to this cluster are shown in table 2 and were identified as n-butyrate, propionate, 3-hydroxyisovalerate, valerate, leucine, isoleucine, alanine, and amide NH-signals of conjugated bile acids. Changes in area intensities for bile acids, valine and methyl malonate are plotted separately. In the case of bile acids,

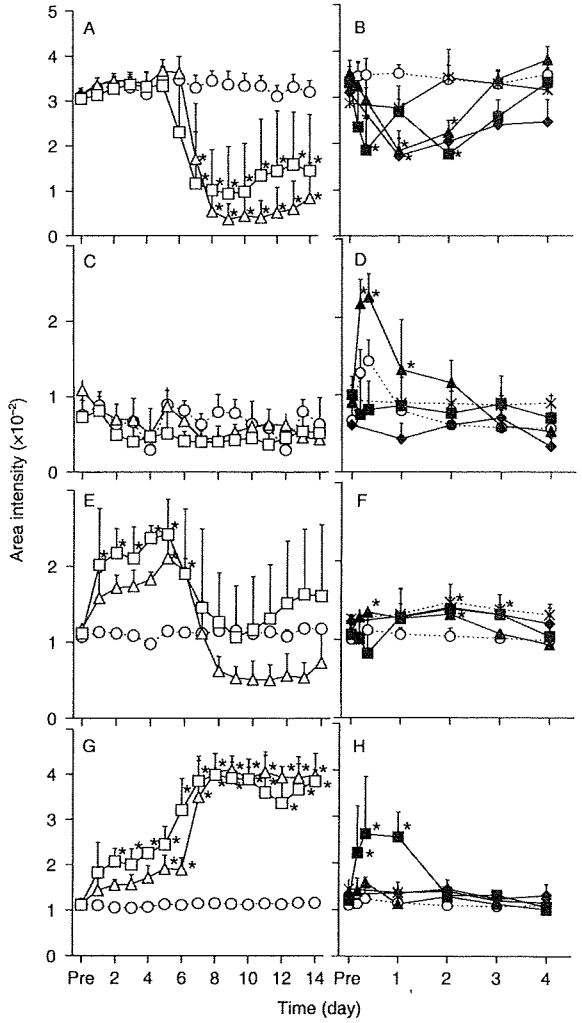

Fig. 4. Change in mean area intensity of chemical shifts for sarcosine (A, B), histidine (C, D), acetoacetate (E, F) and glucose (G, H). Animals treated with: vehicle (O) or cyclosporine A (CyA, △: 10 mg/kg and □: 20 mg/kg, intraperitoneal administration, n = 5) are visualized in A, C, E, and G; vehicle (O), sham operation (×), 4,4′-methylene dianiline (DAPM, ▲: 75 mg/kg, oral administration, n = 5), α-naphthylisothiocyanate (ANIT, ■: 75 mg/kg, oral administration, n = 5), and bile duct ligation (BDL, ◆: n = 3) are visualized in B, D, F, and H. Each point represents means ± S.D. of three or five animals. Significant difference from the control group, *P < 0.05.

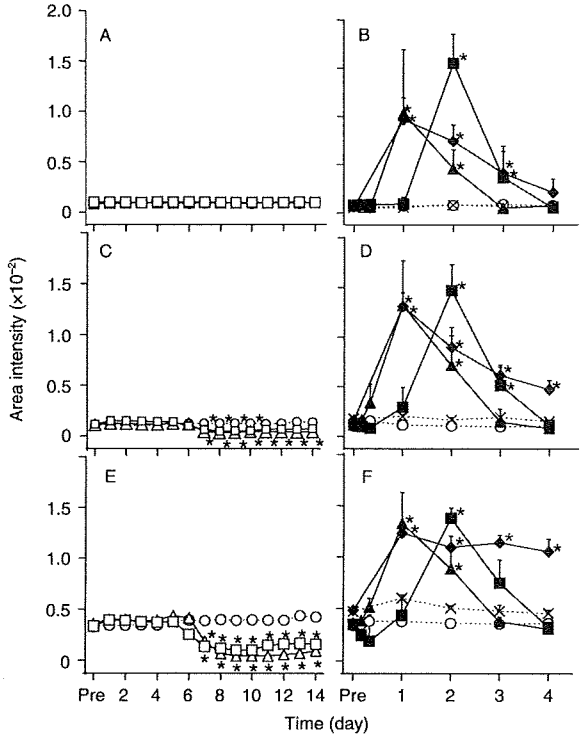

Fig. 5. Change in mean area intensity of chemical shifts for bile acids (A, B), valine (C, D) and methyl malonate (E, F). Animals treated with: vehicle (O) or cyclosporine A (CyA, △: 10 mg/kg and □: 20 mg/kg, intraperitoneal administration, n = 5) are visualized in A, C, and E; vehicle (O), sham operation (×), 4,4′-methylene dianiline (DAPM, ▲: 75 mg/kg, oral administration, n = 5), α-naphthylisothiocyanate (ANIT, ■: 75 mg/kg, oral administration, n = 5), and bile duct ligation (BDL, ◆: n = 3) are visualized in B, D, and F. Each point represents means ± S.D. of three or five animals. Significant difference from the control group, *P < 0.05.

cyclosporine A treatment (fig. 5A) did not affect area intensities, but 4,4′-methylene dianiline, α-naphthylisothiocyanate, and bile duct ligation (fig. 5B) increased it significantly. For valine and methyl malonate, cyclosporine A treatment (fig. 5C and E) decreased area intensities significantly from 7 days compared with control, while 4,4′-methylene dianiline, α-naphthylisothiocyanate and bile duct ligation treatment (figs. 5D and F) increased them.

The sixth cluster, which included acetate, represented the area intensity of chemical shifts unchanged from 1 to 6 days of administration and suppressed thereafter in the cyclosporine A-treated groups, and those enhanced in 4,4′methylene dianiline-, α-naphthylisothiocyanate-, bile duct ligation- and sham operation-treated groups (fig. not shown). The seventh cluster, which included *N*-methylnicotinamide, represented the area intensity of chemical shifts unchanged after treatment of all groups (figure not shown).

Discussion

Hepatotoxicity is the most common complication in drug development, and extensive efforts have been made to minimise the attrition of new drug candidates due to it. Although clinical pathological and histopathological analyses are commonly performed to evaluate hepatotoxicity, new-omics technologies have come to be used increasingly for this purpose.

The purpose of the present study was to determine whether ^{1}H nuclear magnetic resonance-based metabonomics using rat urine samples can discriminate differences in

mechanism of toxicity causing cholestatic injury of the biliary canaliculi or bile ducts. To identify putative metabolites associated with cholestasis, urine samples obtained were subjected to ^{1}H nuclear magnetic resonance analysis.

Previous studies using various types of hepatotoxicants (4,4′-methylene dianiline, clofibrate and galactosamine) suggested that urinary metabolites with chemical shifts of 0.66 to 1.90 ppm were markedly affected by 4,4′-methylene dianiline [12], which is known to induce cholestasis. The dose of 4,4′-methylene dianiline, 250 mg/kg, oral administration, in one previous study was relatively high and might have injured tissues other than the liver [27]. In the present study, area intensities of proton signals from 0.66 to 1.90 ppm (table 2) increased after 4,4′-methylene dianiline treatment in a dose-dependent manner from 50 mg/kg, oral administration (fig. 2), reproducing the findings of previous studies. These results imply that the observed changes in proton signals from 0.66 to 1.90 ppm are closely related to cholestasis. α-Naphthylisothiocyanate is a well-known cholestatic hepatotoxicant and produces cholestasis through injury of epithelial cells of the major bile duct [28]. α-Naphthylisothiocyanate is reported to cause liver injury by a mechanism different from that of 4,4′-methylene dianiline [29], and some differences between 4,4′-methylene dianiline and α-naphthylisothiocyanate treatment may support this (tables 4 and 5). Even if differences do exist in hepatotoxic mechanism between 4,4′-methylene dianiline and α-naphthylisothiocyanate, the two agents produced the same urinary metabolite pattern, suggesting that the changes in urinary metabolites observed were caused by cholestasis itself. The results for α-naphthylisothiocyanate agree with those of previous studies by Beckwith-Hall *et al.* (200 mg/kg, oral administration), Waters *et al.* (150 mg/kg, oral administration), and Schoonen *et al.* (100 mg/kg, oral administration), who reported that bile acids, valine, isoleucine, leucine, and creatine levels were increased in urine [8,30,31]. α-Naphthylisothiocyanate impairs bile flow, resulting in accumulation of bile acids within the bile ducts, and this may lead to bile acid-mediated micellar solubilization of membrane lipids due to a detergent effect in experimental animals [32].

Artificial cholestasis producing permanent obstruction of bile flow has been induced by bile duct ligation [33] and compared with cholestasis induced by chemical substances in rats. Persistent increases in γ-glutamyltranspeptidase, total bilirubin and urinary valine and methyl malonate indicated permanent stasis of bile flow and agreed with a study revealing increase in urinary excretion of bile acids in bile duct ligation-treated rats [34]. Since the change in urinary metabolite profile at 0.66 to 1.90 ppm in the 4,4′-methylene dianiline- and α-naphthylisothiocyanate-treated groups are quite similar to that in animals with bile duct ligation (fig. 5B, D and F), 4,4′-methylene dianiline and α-naphthylisothiocyanate appear to induce cholestasis by obstructing bile flow and thus produce urinary metabolite patterns similar to those obtained with bile duct ligation. As shown in table 5 and fig. 4, although some differences existed among treatments in urinary metabolites, the patterns of changes were not consistent among 4,4′-methylene dianiline, α-naphthylisothiocyanate and bile duct ligation, suggesting that these changes are not specific to cholestasis.

Cyclosporine A was used to inhibit biliary secretion of bile acid, as cyclosporine A is known to cause cholestasis by inhibiting both basal and canalicular hepatocellular bile salt transporters [35,36] and suppressing the bile flow. Although no remarkable histological changes were observed in the cyclosporine A-treated group (table 4), functional impairment of cells in the biliary canaliculi appeared to be induced, as suggested by the increase in serum total bilirubin and total bile acids with cyclosporine A at both 10 and 20 mg/kg. There have also been reports that administration of cyclosporine A at the same doses resulted in significant decrease in bile flow and bile acid secretion [14–16]. Therefore, cyclosporine A was considered to have produced cholestasis as with 4,4′-methylene dianiline, α-naphthylisothiocyanate and bile duct ligation. However, in urinary metabolites, cyclosporine A differed markedly from 4,4′-methylene dianiline, α-naphthylisothiocyanate and bile duct ligation in that it decreased the area intensities of proton signals from 0.66 to 1.90 ppm in urine (fig. 5A, C and E).

The change of urinary metabolites induced by cyclosporine A may be caused by nephrotoxicity, because histological changes characterized by tubular degeneration of the kidneys were noted in the cyclosporine A-treated group (table 4). However, this possibility is not plausible because the characteristic changes of nephrotoxicity in urinary metabolites were not observed in this study. Cyclosporine A is known to injure the proximal tubule cells in rats [37,38]. In previous studies using cyclosporine A at a dose of 45 mg/kg and oral administration for 9 days, Lenz *et al.* reported increases of glucose, acetate, succinate, trimethylamine, lactate, and decreases of citrate, trimethylamine-*N*-oxide [18]. Other nephrotoxic compounds, including hexachlorobutadiene, mercuric chloride, para-aminophenol, sodium fluoride, and uranyl nitrate, which induce the proximal tubule cell injury, are also shown to increase glucose, acetate, succinate, amino acids (alanine, isoleucine, leucine, valine), lactate, *N,N*-dimethylglycine and decrease citrate, 2-oxyglutarate and hippurate in urine by ^{1}H nuclear magnetic resonance analysis [39–43]. Therefore, cyclosporine A at 45 mg/kg, oral administration, is considered to induce changes in urinary metabolites due to nephrotoxicity. However, in the present study, cyclosporine A at 10 and 20 mg/kg, intraperitoneal administration did not increase acetate, succinate, trimethylamine, lactate, nor decrease trimethylamine-*N*-oxide even after 14 days' treatment (table 5), suggesting that the renal function was not impaired as to cause the changes of urinary metabolites, although histological changes was observed.

The change of urinary metabolites by cyclosporine A can be explained as follows. One of the mechanisms of cyclosporine A-induced cholestasis appears to involve inhibition by cyclosporine A of bile acid : CoA ligase activity due to binding at the bile acid binding site [44] and reduction

of production of bile acid conjugates [45]. Bile acids are cytotoxic, but when conjugated become less toxic, and in conjugated form are more amenable to renal excretion. Due to inhibition of formation of conjugated bile acids by cyclosporine A, hepatic uptake and biliary excretion of bile acids will be decreased. Therefore, plasma total bile acids were thought to have increased and excretion of bile acids in urine to have decreased in cyclosporine A-treated rats.

Although the mechanisms responsible for the decreases in urinary leucine, isoleucine, valine, and methyl malonate have yet to be clarified in detail, some reports have suggested relationships between liver diseases and changes in branched-chain amino acids (leucine, isoleucine, and valine). Children with mild-moderate chronic cholestatic liver disease had decreased plasma concentrations of branched-chain amino acids in the presence of increased requirements for total branched-chain amino acids [46,47], suggesting that decreases in plasma branched-chain amino acids levels may be reflective of increases in branched-chain amino acids requirements. Correspondingly, urinary branched-chain amino acids levels are considered to be decreased. There is evidence in animal models of liver disease for increased activity of the branched chain keto-acid dehydrogenase complex in liver, suggesting that increased oxidation of the branched-chain amino acids may occur [48].

The magnitudes of area intensities of proton signals derived from 0.66 to 1.90 ppm appear to be altered differently by intra-hepatic and extra-hepatic cholestatic injury caused by cyclosporine A and, 4,4′-methylene dianiline, α-naphthylisothiocyanate or bile duct ligation, respectively, and are thus likely to be useful as biomarkers in urine. We conclude that a bunch of bile acids, valine, and methyl malonate have a possibility to be biomarkers of cholestasis distinguishing a difference in mechanism of toxicity when analysed with data serum bilirubin. ^{1}H nuclear magnetic resonance metabonomics technology appears to be very useful as a means of detecting cholestatic liver injury. Other compounds, like nephrotoxic ones, are also shown to increase amino acids (alanine, isoleucine, leucine, valine) in urine by ^{1}H nuclear magnetic resonance analysis [10,41,42]. Therefore, further studies should be directed toward assessing the endogenous metabolites which can be used as biomarkers to differentiate cholestatic injury from other diseases.

^{1}H nuclear magnetic resonance-based metabonomics can be used to address a large range of preclinical and clinical problems. This study has established the importance of metabonomics technology in examination of the mechanistic complexity of drug toxicity as well as the benefits of this approach in drug safety evaluation and biomarker discovery for drug development.

Acknowledgement

The authors would like to thank all those involved in the performance of this study at Tsukuba Research and Kawashima Research, Drug Safety Research Laboratories, Eisai, with special thanks to Dr. N. Toritsuka, K. Asai, and T. Imade.

References

1 Kola I, Landis J. Can the pharmaceutical industry reduce attrition rates? Nat Rev Drug Discov 2004;**3**:711–5.
2 Steiner G, Suter L, Boess F, Gasser R, de Vera MC, Albertini S *et al.* Discriminating different classes of toxicants by transcript profiling. Environ Health Perspect 2004;**112**:1236–48.
3 Lewis JH, Zimmerman HJ. Drug- and chemical-induced cholestasis. Clin Liver Dis 1999;**3**:433–64.
4 Trauner M, Meier PJ, Boyer JL. Molecular pathogenesis of cholestasis. N Engl J Med 1998;**339**:1217–27.
5 Chitturi S, Farrell GC. Drug-induced cholestasis. Semin Gastrointest Dis 2001;**12**:113–24.
6 Rodriguez-Garay EA. Cholestasis: human disease and experimental animal models. Ann Hepatol 2003;**2**:150–8.
7 Zollner G, Trauner M. Molecular mechanisms of cholestasis. Wien Med Wochenschr 2006;**156**:380–5.
8 Beckwith-Hall BM, Nicholson JK, Nicholls AW, Foxall PJ, Lindon JC, Connor SC *et al.* Nuclear magnetic resonance spectroscopic and principal components analysis investigations into biochemical effects of three model hepatotoxins. Chem Res Toxicol 1998;**11**:260–72.
9 Holmes E, Nicholls AW, Lindon JC, Ramos S, Spraul M, Neidig P *et al.* Development of a model for classification of toxin-induced lesions using ^{1}H NMR spectroscopy of urine combined with pattern recognition. NMR Biomed 1998;**11**:235–44.
10 Robertson DG, Reily MD, Sigler RE, Wells DF, Paterson DA, Braden TK. Metabonomics: evaluation of nuclear magnetic resonance (NMR) and pattern recognition technology for rapid in vivo screening of liver and kidney toxicants. Toxicol Sci 2000;**57**:326–37.
11 Coen M, Holmes E, Lindon JC, Nicholson JK. NMR-based metabolic profiling and metabonomic approaches to problems in molecular toxicology. Chem Res Toxicol 2008;**21**:9–27.
12 Ishihara K, Katsutani N, Aoki T. A metabonomics study of the hepatotoxicants galactosamine, methylene dianiline and clofibrate in rats. Basic Clin Pharmacol Toxicol 2006;**99**:251–60.
13 Kanz MF, Gunasena GH, Kaphalia L, Hammond DK, Syed YA. A minimally toxic dose of methylene dianiline injures biliary epithelial cells in rats. Toxicol Appl Pharmacol 1998;**150**:414–26.
14 Stone BG, Udani M, Sanghvi A, Warty V, Plocki K, Bedetti CD *et al.* Cyclosporin A-induced cholestasis. Gastroenterology 1987;**93**:344–51.
15 Deters M, Klabunde T, Kirchner G, Resch K, Kaever V. Sirolimus/cyclosporine/tacrolimus interactions on bile flow and biliary excretion of immunosuppressants in a subchronic bile fistula rat model. Br J Pharmacol 2002;**136**:604–12.
16 Galan AI, Fernandez E, Moran D, Munoz ME, Jimenez R. Cyclosporine A hepatotoxicity: effect of prolonged treatment with cyclosporine on biliary lipid secretion in the rat. Clin Exp Pharmacol Physiol 1995;**22**:260–5.
17 McCarthy DJ, Struck RF, Shih TW, Suling WJ, Hill DL, Enke SE. Disposition and metabolism of the carcinogen reduced Michler's ketone in rats. Cancer Res 1982;**42**:3475–9.
18 Lenz EM, Bright J, Knight R, Wilson ID, Major H. Cyclosporin A-induced changes in endogenous metabolites in rat urine: a metabonomic investigation using high field ^{1}H NMR spectroscopy, HPLC-TOF/MS and chemometrics. J Pharm Biomed Anal 2004;**35**:599–608.
19 Weljie AM, Newton J, Mercier P, Carlson E, Slupsky CM. Targeted profiling: quantitative analysis of ^{1}H NMR metabolomics data. Anal Chem 2006;**78**:4430–42.
20 Saude EJ, Slupsky CM, Sykes BD. Optimization of NMR analysis of biological fluids for quantitative accuracy. Metabolomics 2006;**2**:113–23.

21 Saude EJ, Sykes BD. Urine stability for metabolomic studies: effects of preparation and storage. Metabolomics 2007;**3**:19–27.
22 Schnackenberg LK, Dragan YP, Reilly MD, Robertson DG, Beger RD. Evaluation of NMR spectral data of urine in conjunction with measured clinical chemistry and histopathology parameters to assess the effects of liver and kidney toxicants. Metabolomics 2007;**3**:87–100.
23 Shearer J, Duggan G, Weljie A, Hittel DS, Wasserman DH, Vogel HJ. Metabolomic profiling of dietary-induced insulin resistance in the high fat-fed C57BL/6J mouse. Diabetes Obes Metab 2008;**10**:950–8.
24 Nicholson JK, Wilson ID. High resolution proton magnetic resonance spectroscopy of biological fluids. Prog Nuclear Magn Reson Spectrosc 1989;**21**:449–501.
25 Lindon JC, Nicholson JK, Everett JR. NMR spectroscopy of biofluids. Ann Rep NMR Spectrosc 1999;**38**:1–88.
26 Ijare OB, Somashekar BS, Gowda GA, Sharma A, Kapoor VK, Khetrapal CL. Quantification of glycine and taurine conjugated bile acids in human bile using ^{1}H NMR spectroscopy. Magn Reson Med 2005;**53**:1441–6.
27 Kanz MF, Kaphalia L, Kaphalia BS, Romagnoli E, Ansari GA. Methylene dianiline: acute toxicity and effects on biliary function. Toxicol Appl Pharmacol 1992;**117**:88–97.
28 Jean PA, Roth RA. Naphthylisothiocyanate disposition in bile and its relationship to liver glutathione and toxicity. Biochem Pharmacol 1995;**50**:1469–74.
29 Kanz MF, Dugas TR, Liu H, Santa Cruz V. Glutathione depletion exacerbates methylenedianiline toxicity to biliary epithelial cells and hepatocytes in rats. Toxicol Sci 2003;**74**:447–56.
30 Waters NJ, Holmes E, Williams A, Waterfield CJ, Farrant RD, Nicholson JK. NMR and pattern recognition studies on the time-related metabolic effects of α-naphthylisothiocyanate on liver, urine, and plasma in the rat: an integrative metabonomic approach. Chem Res Toxicol 2001;**14**:1401–12.
31 Schoonen WG, Kloks CP, Ploemen JP, Smit MJ, Zandberg P, Horbach GJ *et al.* Uniform procedure of ^{1}H NMR analysis of rat urine and toxicometabonomics Part II: comparison of NMR profiles for classification of hepatotoxicity. Toxicol Sci 2007;**98**:286–97.
32 Wang GF, Stacey NH. Elevation of individual serum bile acids on exposure to trichloroethylene or α-naphthylisothiocyanate. Toxicol Appl Pharmacol 1990;**105**:209–15.
33 Kinugasa T, Uchida K, Kadowaki M, Takase H, Nomura Y, Saito Y. Effect of bile duct ligation on bile acid metabolism in rats. J Lipid Res 1981;**22**:201–7.
34 Takada Y, Sano N, Takikawa H. Urinary excretion of bile acids in bile duct-ligated rats. J Gastroenterol 2003;**38**:561–6.
35 Stacey NH, Kotecka B. Inhibition of taurocholate and ouabain transport in isolated rat hepatocytes by cyclosporin A. Gastroenterology 1988;**95**:780–6.
36 Bohme M, Jedlitschky G, Leier I, Buchler M, Keppler D. ATP-dependent export pumps and their inhibition by cyclosporins. Adv Enzyme Regul 1994;**34**:371–80.
37 Farthing MJ, Clark ML. Nature of the toxicity of cyclosporin A in the rat. Biochem Pharmacol 1981;**30**:3311–6.
38 Jackson NM, Hsu CH, Visscher GE, Venkatachalam MA, Humes HD. Alterations in renal structure and function in a rat model of cyclosporine nephrotoxicity. J Pharmacol Exp Ther 1987;**242**:749–56.
39 Gartland KP, Bonner FW, Nicholson JK. Investigations into the biochemical effects of region-specific nephrotoxins. Mol Pharmacol 1989;**35**:242–50.
40 Bairaktari E, Katopodis K, Siamopoulos KC, Tsolas O. Paraquat-induced renal injury studied by ^{1}H nuclear magnetic resonance spectroscopy of urine. Clin Chem 1998;**44**:1256–61.
41 Shockcor JP, Holmes E. Metabonomic applications in toxicity screening and disease diagnosis. Curr Top Med Chem 2002;**2**:35–51.
42 Gibbs A. Comparison of the specificity and sensitivity of traditional methods for assessment of nephrotoxicity in the rat with metabonomic and proteomic methodologies. J Appl Toxicol 2005;**25**:277–95.
43 Waters NJ, Waterfield CJ, Farrant RD, Holmes E, Nicholson JK. Metabonomic deconvolution of embedded toxicity: application to thioacetamide hepato- and nephrotoxicity. Chem Res Toxicol 2005;**18**:639–54.
44 Vessey DA, Kelley M. Inhibition of bile acid conjugation by cyclosporin A. Biochim Biophys Acta 1995;**1272**:49–52.
45 Moran D, De Buitrago JM, Fernandez E, Galan AI, Munoz ME, Jimenez R. Inhibition of biliary glutathione secretion by cyclosporine A in the rat: possible mechanisms and role in the cholestasis induced by the drug. J Hepatol 1998;**29**:68–77.
46 Chin SE, Shepherd RW, Thomas BJ, Cleghorn GJ, Patrick MK, Wilcox JA *et al.* Nutritional support in children with end-stage liver disease: a randomized crossover trial of a branched-chain amino acid supplement. Am J Clin Nutr 1992;**56**:158–63.
47 Mager DR, Wykes LJ, Roberts EA, Ball RO, Pencharz PB. Branched-chain amino acid needs in children with mild-to-moderate chronic cholestatic liver disease. J Nutr 2006;**136**:133–9.
48 Honda T, Fukuda Y, Nakano I, Katano Y, Goto H, Nagasaki M *et al.* Effects of liver failure on branched-chain α-keto acid dehydrogenase complex in rat liver and muscle: comparison between acute and chronic liver failure. J Hepatol 2004;**40**:439–45.

0090-9556/09/3702-345–351$20.00
DRUG METABOLISM AND DISPOSITION

DMD 37:345–351, 2009

Vol. 37, No. 2
24521/3429942
Printed in U.S.A.

DMD

DRUG METABOLISM AND DISPOSITION

Metabolic Activation of Benzodiazepines by CYP3A4[S]

Katsuhiko Mizuno, Miki Katoh,[1] Hirotoshi Okumura, Nao Nakagawa, Toru Negishi, Takanori Hashizume, Miki Nakajima, and Tsuyoshi Yokoi

Drug Metabolism and Toxicology, Faculty of Pharmaceutical Sciences, Kanazawa University, Kanazawa, Japan (K.M., M.K., H.O., N.N., M.N., T.Y.); and Pharmacokinetics Research Laboratories, Dainippon Sumitomo Pharma Co., Ltd., Osaka, Japan (T.N., T.H.)

Received September 15, 2008; accepted November 10, 2008

ABSTRACT:

Cytochrome P450 3A4 is the predominant isoform in liver, and it metabolizes more than 50% of the clinical drugs commonly used. However, CYP3A4 is also responsible for metabolic activation of drugs, leading to liver injury. Benzodiazepines are widely used as hypnotics and sedatives for anxiety, but some of them induce liver injury in humans. To clarify whether benzodiazepines are metabolically activated, 14 benzodiazepines were investigated for their cytotoxic effects on HepG2 cells treated with recombinant CYP3A4. By exposure to 100 μM flunitrazepam, nimetazepam, or nitrazepam, the cell viability in the presence of CYP3A4 decreased more than 25% compared with that of the control. In contrast, in the case of other benzodiazepines, the changes in the cell viability between CYP3A4 and control Supersomes were less than 10%. These results suggested that nitrobenzodiazepines such as flunitrazepam, nimetazepam, and nitrazepam were metabolically activated by CYP3A4, which resulted in cytotoxicity. To identify the reactive metabolite, the glutathione adducts of flunitrazepam and nimetazepam were investigated by liquid chromatography-tandem mass spectrometry. The structural analysis for the glutathione adducts of flunitrazepam indicated that a nitrogen atom in the side chain of flunitrazepam was conjugated with the thiol of glutathione. Therefore, the presence of a nitro group in the side chain of benzodiazepines may play a crucial role in the metabolic activation by CYP3A4. The present study suggested that metabolic activation by CYP3A4 was one of the mechanisms of liver injury by nitrobenzodiazepines.

Drug-induced hepatotoxicity is one of the major causes of liver injury and is classified into intrinsic and idiosyncratic types. Intrinsic drug reactions can occur in a dose-dependent manner in any individual and are reproducible in preclinical studies. In contrast, idiosyncratic drug reactions do not occur in most patients at any dose, and they are often referred to as rare, with a typical incidence of from 1/100 to 1/100,000 (Uetrecht, 1999). Because idiosyncratic drug reactions are difficult to spot during drug development, some drugs launched on the market were later withdrawn because of idiosyncratic hepatotoxicity. Such drugs withdrawn for hepatotoxicity are known to produce reactive metabolites (Guengerich and MacDonald, 2007). The generation of reactive metabolites may relate to the formation of free radicals, oxidation of thiol, and covalent binding with endogenous macromolecules, resulting in the oxidation of cellular components or inhibition of normal cellular function (Guengerich and Liebler, 1985).

The generation of a reactive metabolite catalyzed by drug-metabolizing enzymes such as cytochrome P450 (P450) is defined as metabolic activation. P450 is the major drug-metabolizing enzyme that is highly expressed in human liver. CYP3A4 is the predominant isoform in liver (Shimada et al., 1994) and metabolizes more than 50% of the clinical drugs commonly used (Guengerich, 1995). However, CYP3A4 is also responsible for the formation of reactive metabolites of flutamide (Berson et al., 1993), trazodone (Kalgutkar et al., 2005), and troglitazone (Yamamoto et al., 2002). It is suggested that the reactive metabolites of flutamide, trazodone, and troglitazone cause the idiosyncratic hepatotoxicity in humans.

Prediction of the metabolic activation and the cytotoxicity of drug candidates is necessary in drug development. Human hepatocarcinoma HepG2 cells are commonly used for predicting hepatotoxicity in vitro. However, low expression levels of P450s in HepG2 cells may be responsible for the fact that 30% of the compounds were falsely classified as nontoxic (Rodriguez-Antona et al., 2002; Wilkening et al., 2003; Hewitt and Hewitt, 2004). In a recent study, a useful in vitro cell-based assay made by combining recombinant CYP3A4 with HepG2 cells was established (Vignati et al., 2005). It was demonstrated that hepatotoxicants whose reactive metabolites were generated by CYP3A4 exhibited cytotoxicity to the HepG2 cells. This assay system could be applied to screen for hepatotoxicity by drugs.

This study was supported by Young Scientists of the Ministry of Education, Culture, Sports, Science and Technology of Japan [Grant 19790120]; and Ministry of Health, Labor, and Welfare, Health and Labor Science Research [Grant H20-BI-001].

K.M. and M.K. contributed equally to this work.

[1] Current affiliation: Faculty of Pharmacy, Meijo University, Tempaku-ku, Nagoya, Japan.

Article, publication date, and citation information can be found at http://dmd.aspetjournals.org.

doi:10.1124/dmd.108.024521.

[S] The online version of this article (available at http://dmd.aspetjournals.org) contains supplemental material.

ABBREVIATIONS: P450, cytochrome P450; MTT, 3-(4,5-dimetylthiazol-2-yl)-2,5-diphenyl tetrazolium bromide; LC, liquid chromatography; MS/MS, tandem mass spectrometry; MS, mass spectrometry; LCMS-IT-TOF, liquid chromatography ion trap and time-of-flight mass spectrometry.

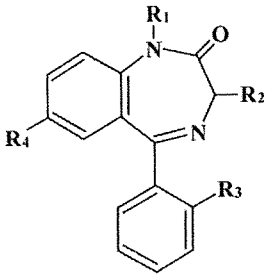

Benzodiazepine	R_1	R_2	R_3	R_4
Clonazepam	H	H	Cl	NO_2
Desmethyldiazepam	H	H	H	Cl
Diazepam	CH_3	H	H	Cl
Flunitrazepam	CH_3	H	F	NO_2
Flurazepam	$CH_2CH_2N(C_2H_5)$	H	F	Cl
Lorazepam	H	OH	Cl	Cl
Nimetazepam	CH_3	H	H	NO_2
Nitrazepam	H	H	H	NO_2
Norfludiazepam	H	H	F	Cl
Oxazepam	H	OH	H	Cl
Temazepam	CH_3	OH	H	Cl

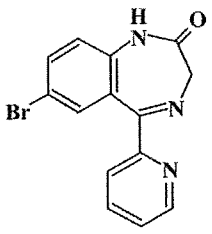

Bromazepam

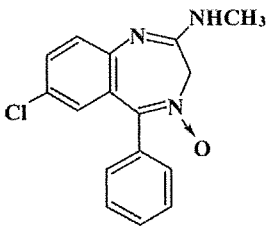

Chlordiazepoxide

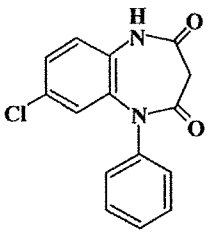

Clobazam

FIG. 1. Chemical structures of the 14 benzodiazepines used in the present study.

Benzodiazepines have been used extensively as hypnotics and sedatives for anxiety throughout the world. The mechanism of their efficacy is to amplify the action of γ-aminobutyric acid by acting as agonists at γ-aminobutyric acid receptors (Costa et al., 2002). Many benzodiazepines have been launched on the market and used in clinical practice. Two of the major benzodiazepines, flunitrazepam and nitrazepam, are widely used as hypnotic and anesthetic premedications in Europe and Japan. In 2001, it was announced by the Ministry of Health, Labor and Welfare of Japan that flunitrazepam induced hepatotoxicity. Chronic administration of antidepressant drugs including nitrazepam was reported to induce severe hepatic disorders (Seki et al., 2008). Clonazepam is one of the benzodiazepines used as an anxiolytic and anticonvulsant in clinical practice. Hepatic injury was reported to occur after treatment with clonazepam for 6 weeks in Ethiopia (Olsson and Zettergren, 1988).

The purpose of the present study was to clarify whether the metabolic activation of benzodiazepines by P450 occurs, leading to the hepatotoxicity. We investigated the cell viability in HepG2 cells in the presence or absence of CYP3A4 after exposure to 14 commercially available benzodiazepines (Fig. 1). There are many structural analogs of benzodiazepines, and the chemical structures and cytotoxicity in HepG2 cells were compared.

Materials and Methods

Materials. Clonazepam, clobazam, diazepam, lorazepam, nimetazepam, nitrazepam, and oxazepam were obtained from Wako Pure Chemicals (Osaka, Japan). Bromazepam, chlordiazepoxide, desmethyldiazepam, flunitrazepam, flurazepam, norfludiazepam, and temazepam were purchased from Sigma-Aldrich (St. Louis, MO). Human CYP2C9, 2C19, and 3A4 Supersomes (recombinant cDNA-expressed P450 enzymes prepared from a baculovirus insect cell system) and control Supersomes were purchased from BD Gentest (Woburn, MA). These microsomes coexpressed NADPH-cytochrome P450 reductase and cytochrome b_5. All other reagents used in this study were of the highest or analytical grade commercially available.

Cell Culture. Human hepatocarcinoma cell line HepG2 was obtained from Riken Gene Bank (Tsukuba, Japan). The cells were cultured in Dulbecco's modified Eagle's medium (Nissui Pharmaceutical, Tokyo, Japan) supplemented with 10% fetal bovine serum (Invitrogen, Melbourne, Australia) and 0.1 mM nonessential amino acids (Invitrogen) at 37°C in an atmosphere of 5% CO_2 and 95% air.

Cell Viability Assay. HepG2 cells were seeded at a density of 1×10^4 cells/well in 96-well plates with medium containing 3% fetal bovine serum, benzodiazepines, 8 nM human CYP2C9, CYP2C19, CYP3A4, or control Supersomes and 1 mM NADPH and then incubated at 37°C for 24 h. In the preliminary study, we investigated the cell viability in HepG2 cells with various P450 concentrations and incubation time. The 8 nM P450 and 24-h incubation were enough to detect cytotoxicity in this assay system. The final concentration of organic solvent (dimethyl sulfoxide) in medium was less than 0.2%. Cell viability after a 24-h incubation was evaluated by the intracellular ATP concentration using a CellTiter-Glo Luminescent Cell Viability Assay (ATP assay; Promega, Madison, WI) and 3-(4,5-dimetylthiazol-2-yl)-2,5-diphenyl tetrazolium bromide (MTT) activities using a CellTiter-Blue Cell Viability Assay (MTT assay; Promega). According to the protocols of the manufacturer, the luminescence of the generated oxyluciferin was measured in the ATP assay and the fluorescence of the generated resorufin was detected fluorometrically (excitation: 338 nm, emission: 458 nm) in the MTT assay by using a 1420 ARVO MX luminometer (PerkinElmer Wallac, Turku, Finland).

Caspase Assay. HepG2 cells were seeded under the same conditions and incubated at 37°C for 24 h. After incubation, the caspase 3/7 activity was measured using a Caspase-Glo 3/7 Assay (Promega) according to the protocol of the manufacturer. The luminescence of the generated aminoluciferin was measured using a 1420 ARVO MX luminometer.

Detection of Glutathione Adducts. A typical reaction mixture (final volume of 0.25 ml) contained 50 nM human CYP3A4 Supersomes, 100 mM potassium phosphate buffer (pH 7.4), an NADPH-generating system consisting of 0.775 mM nicotinamide adenine dinucleotide phosphate (oxidized form), 0.165 mM glucose 6-phosphate, 0.165 mM $MgCl_2$, 0.2 unit/ml glucose-6-phosphate dehydrogenase, 10 mM glutathione (reduced form), and 100 μM benzodiazepines (flunitrazepam, nimetazepam, nitrazepam, bromazepam, or temazepam). The final concentration of dimethyl sulfoxide in the reaction mixture was less than 1%. Incubation was performed at 37°C for 60 min and terminated by adding 0.75 ml of ice-cold methanol. After centrifugation at 15,000*g*, the supernatant was subjected to liquid chromatography-tandem mass spectrometry (LC-MS/MS) (API 4000; Applied Biosystems, Foster City, CA). An LC-10 liquid chromatograph (Shimadzu, Kyoto, Japan) was used with an Inertsil ODS-3 analytical column (2.1 × 100 mm, 3 μm; GL Science, Tokyo, Japan). The column temperature was 40°C. The mobile phase was 10 mM ammonium acetate buffer (pH 4.0) (A) and acetonitrile (B). The conditions for

elution were as follows: 5 to 90% B (0–6 min), 90% B (6–11 min), 90 to 5% B (11–11.01 min), and 5% B (11.01–15 min). Linear gradients were used for all solvent changes. The flow rate was 0.2 ml/min. The liquid chromatograph was connected to an API 4000 mass spectrometer operated in the negative electrospray ionization mode. The turbo gas was maintained at 450°C. Air was used as the nebulizing and turbo gas at 60 psi. Nitrogen was used as the curtain gas at 20 psi. The collision energy was −50 V. The *m/z* 300 to 850 was scanned at the precursor ion (*m/z* 272; major mass spectrum fragment of glutathione).

Identification of Glutathione Adducts. Liquid chromatography ion trap and time-of-flight mass spectrometry (LCMS-IT-TOF) (Shimadzu) was used to identify the structures of the glutathione adducts of the nitrobenzodiazepines. The incubation mixture was the same as that described above except for CYP3A4 Supersomes (100 nM). Flunitrazepam and nimetazepam were used as test compounds. After centrifugation at 15,000*g* for 5 min, the supernatant was subjected to LCMS-IT-TOF using an Inertsil ODS-3 analytical column (2.1 × 100 mm, 3 μm). The LC conditions were the same as described earlier. The turbo gas was maintained at 450°C. Air was used as the nebulizing and turbo gas at 60 psi. Nitrogen was used as the curtain gas at 20 psi. The collision energy was 50 V. Structure analysis of the glutathione adducts of flunitrazepam and nimetazepam was performed by scanning at the product ion (*m/z* 621 and *m/z* 603, respectively) in the positive electrospray ionization mode.

Statistics. Data are expressed as mean ± S.D. ($n = 3$). Two groups were compared with a two-tailed Student's *t* test. $P < 0.05$ was considered statistically significant.

Results

Cell Viability of HepG2 Cells Treated with CYP3A4 and Benzodiazepines. HepG2 cells were incubated for 24 h with the 14 benzodiazepines at 50, 100, 200, and 400 μM in the presence of CYP3A4 or control Supersomes and then the cell viability was measured by the ATP and MTT assays. With exposure to 100 μM flunitrazepam, nimetazepam, and nitrazepam, cell viability in the presence of CYP3A4 Supersomes decreased more than 25% than with control Supersomes (Fig. 2). Although clonazepam could be dissolved up to 100 μM in the reaction mixtures, the viability of HepG2 cells treated with CYP3A4 Supersomes and 100 μM clonazepam exhibited 57 and 35% decreases in the ATP and MTT assays, respectively, compared with viability with control Supersomes (Supplemental Fig. 2). Flunitrazepam, nimetazepam, nitrazepam, and clonazepam are nitrobenzodiazepines that have a nitro group at the 7-position (Fig. 1). In contrast, for the other 10 benzodiazepines (bromazepam, chlordiazepoxide, clobazam, desmethyldiazepam, diazepam, flurazepam, lorazepam, norfludiazepam, oxazepam, and temazepam) at 100 μM, the changes in cell viability between CYP3A4 and control Supersomes were less than 10% and much smaller than those for the nitrobenzodiazepines (Fig. 2 and Supplemental Fig. 1). Moreover, 25% effective concentrations (EC_{25}) of nitrobenzodiazepines were less than 100 μM, and EC_{25} values of all other benzodiazepines were more than 300 μM in the ATP assay (Supplemental Table 1). Desmethyldiazepam, diazepam, flurazepam, lorazepam, norfludiazepam, and oxazepam exhibited concentration-dependent cytotoxicity in HepG2 cells incubated both with and without CYP3A4 (Fig. 2 and Supplemental Fig. 1).

Cell Viability on HepG2 Cells Treated with CYP2Cs and Nitrobenzodiazepines. It has been reported that CYP2C9 and CYP2C19 are involved in the metabolism of flunitrazepam (Hesse et al., 2001; Kilicarslan et al., 2001). Therefore, we investigated whether CYP2C9 and CYP2C19 affect the cytotoxicity caused by nitrobenzodiazepines in HepG2 cells. As shown in Fig. 3, the differences in the cell viability between CYP2Cs and control Supersomes when exposed to 100 μM nitrobenzodiazepines were less than 10%.

Caspase 3/7 Activity in HepG2 Cells Treated with CYP3A4 and Nitrobenzodiazepines. As a key factor of apoptosis, the caspase 3/7 activity was measured in HepG2 cells treated with CYP3A4 and the nitrobenzodiazepines for 24 h. Flunitrazepam, nimetazepam, and nitrazepam significantly increased the caspase 3/7 activities in HepG2 cells in the presence of CYP3A4 Supersomes (Fig. 4, A–C). In contrast, bromazepam as the negative control had no effects on the caspase 3/7 activities both with and without CYP3A4 (Fig. 4D).

Detection of Glutathione Adducts of Benzodiazepines. The glutathione adducts of benzodiazepines were investigated by the negative ion mode of LC-MS/MS. The nitrobenzodiazepines (flunitrazepam, nimetazepam, and nitrazepam) and the negative controls (bromazepam and temazepam) were measured. As shown in Fig. 5, the glutathione adducts of flunitrazepam and nimetazepam were detected in the presence of CYP3A4 Supersomes by precursor ion scans at *m/z* 619 and *m/z* 601 ($[M - H]^-$), respectively. In contrast, there were no adducts of flunitrazepam and nimetazepam when they were used in the control Supersomes (data not shown). In nitrazepam, bromazepam, and temazepam, glutathione adducts were not detected in the presence and absence of CYP3A4.

Identification of Glutathione Adducts of Flunitrazepam and Nimetazepam. The structures of the glutathione adducts of flunitrazepam and nimetazepam were estimated by the positive ion mode of LCMS-IT-TOF. For of the glutathione adduct of flunitrazepam, the product ion mass spectrum of *m/z* 621 ($[M + H]^+$) gave fragment ions at *m/z* 284.1, *m/z* 348.1, and *m/z* 492.1. The molecule weight of the $[M + H]^+$ fragment ion (*m/z* 492.1) meant that it was produced by the molecule weight of the compound (491) and that of a hydrogen ion (H^+; 1). The possible structure of the glutathione adduct of flunitrazepam is shown in Fig. 6. A reactive metabolite of flunitrazepam, in which the nitro group might be metabolized into the amino group, was conjugated to the 7-substituent group by glutathione.

On the other hand, the $[M + H]^+$ ion of the glutathione adduct of nimetazepam (*m/z* 603) gave fragment ions at *m/z* 266.4 and *m/z* 474.2 (Supplemental Fig. 3). The fragment ions at *m/z* 266.4 and *m/z* 474.2 were $[M + H - 337]^+$ and $[M + H - 129]^+$, respectively, corresponding to the fragment ions at *m/z* 284.1 and *m/z* 492.1 obtained from the glutathione adduct of flunitrazepam (*m/z* 621).

Discussion

In the present study, 14 benzodiazepine analogs were investigated for cytotoxic effects resulting from metabolic activation by CYP3A4. The major metabolic pathways of diazepam are 3-hydroxylayion by CYP3A4 and *N*-desmethylation by CYP2C9 (Schwartz et al., 1965; Ono et al., 1996). Thus, desmethyldiazepam, temazepam, and oxazepam are metabolites of diazepam (Fig. 1). In addition, norfludiazepam and nitrazepam would be the metabolites of flurazepam and nimetazepam, respectively.

The cytotoxicity of flunitrazepam, nimetazepam, nitrazepam, and clonazepam was observed in the presence of CYP3A4 Supersomes in HepG2 cells (Fig. 2 and Supplemental Fig. 1), suggesting that these three drugs are metabolically activated by CYP3A4. Flunitrazepam, nimetazepam, nitrazepam, and clonazepam are classified as nitrobenzodiazepines that have a nitro group in the side chain. In contrast, the other 10 benzodiazepines exhibited less cytotoxicity than the nitrobenzodiazepines (Fig. 2 and Supplemental Fig. 1; Supplemental Table 1). In the present study, we first clarified that the presence of a nitro group in the side chain of benzodiazepines may play a crucial rule in the metabolic activation by CYP3A4. To prevent the cytotoxicity by reactive metabolites in the medium, the effects of 200 μM or 1 mM glutathione (reduced form) were measured in this cell viability assay as a preliminary experiment. The glutathione recovered 10% of cell viability in HepG2 cells treated with CYP3A4 and 100 μM flunitraz-